European Organisation
for Astronomical
Research in the
Southern Hemisphere

Organisation Européenne
pour des Recherches
Astronomiques
dans l'Hémisphère Austral

Europäische Organisation
für astronomische
Forschung in der
südlichen Hemisphäre

E-ELT PROGRAMME

THE E-ELT DESIGN REFERENCE MISSION: TECHNICAL DATA USED FOR SIMULATIONS

E-TRE-ESO-080-0718 Issue 1

30 June 2010

Owner	J. Liske		
Project scientist	M. Kissler-Patig		
Head of Programme Office	R. Gilmozzi		
	Name	Date	Signature

Authors

Name	Affiliation
J. Liske	ESO

Change record

Issue	Date	Section / Paragraph affected	Reason / Initiation Documents / Remarks
1	30 June 2010	All	Initial version

Contents

1 Scope

This document describes the technical data and exposure time calculators that were used in simulations for the E-ELT Design Reference Mission during the detailed design phase of the telescope.

2 Applicable documents

2.1 Applicable documents

The following applicable documents form a part of the present document to the extent specified herein. In the event of conflict between applicable documents and the content of the present document, the content of the present document shall be taken as superseding.

AD1 E-ESO-SPE-313-0066 Issue 2, Common definitions and acronyms
AD2 E-TDP-ESO-080-0830 Issue 1, The E-ELT Design Reference Mission: technical data used for simulations – data files

2.2 Reference documents

RD1 E-TRE-ESO-080-0717 Issue 1, The E-ELT Design Reference Mission
RD2 EFP7-TRE-ESO-04000-0002 Issue 1, Report on the impact of instrumentation on the Design Reference Mission

3 Introduction

The E-ELT Design Reference Mission (DRM, [RD1]) encompasses a detailed, hands-on exploration of a selected sample of science cases through the analysis of simulated E-ELT data. These scientific performance simulations for the E-ELT required a large number of inputs regarding the characteristics of the telescope, the instruments, the AO performance, etc. Here we provide a detailed description of the technical input data set that was used for most of the DRM simulations. The data themselves are published as [AD2].

Note that the technical data described here are not meant to be a complete and perfectly accurate representation of the entire E-ELT system in its final design. Instead, we tried to capture only the essential features that affect the system performance, and the information given here merely represents all of the data we were able to compile at the beginning of the DRM process. Where information was missing simplifying (but reasonable) assumptions were made, while some aspects were only covered somewhat rudimentarily. Any possible future work on E-ELT performance simulations should begin by updating this document and aligning it with the final design of the E-ELT system.

The information presented here was originally published as an online technical data repository (where it was also available to the community).

This document also provides descriptions of two online exposure time calculators (ETCs) which were used in the analyses of some of the DRM science cases.

4 Site

Two different sites are considered. Their characteristics are listed in Table 4.1.

Table 4.1: Site parameters.

Site	Altitude [m]	Temperature [K]	Pressure [mb]	PWV [mm]
Paranal-like	2600	285	743	2.3
High & Dry	5000	270	540	0.5

5 Background model

The background brightness and its dependence on wavelength are modelled in the following way:

$$F_{\rm bkg} = {\rm cont}(\lambda) + {\rm em.\ lines}(\lambda) + {\rm atm}(\lambda) + {\rm tel}(\lambda) \tag{5.1}$$

i.e. as the sum of a (pseudo-)continuum, emission lines, thermal atmospheric emission and thermal emission from the telescope (and instrument). Below each of these components is discussed in turn. Atmospheric extinction is also discussed here.

5.1 Continuum

In the blue-optical the background brightness is dominated by the continuum which has contributions from a number of sources, chiefly: diffuse galactic emission, zodiacal light and moonlight scattered by the atmosphere. Hence, in practice the background brightness at a given wavelength and at a given position in the sky depends on a number of parameters, including the position's location with respect to the galaxy, ecliptic and moon, the moon phase, the phase of the solar cycle, the season, the observatory's geomagnetic latitude and airmass. Compared to the darkest possible background most of these systematic effects increase the background by up to several tenths of a magnitude. The moon has the largest effect – up to several magnitudes in the blue. In addition, even when all known systematic effects are accounted for, the background brightness still fluctuates by $\sim$0.2 mag on timescales of minutes, hours and nights. Unfortunately, even if we concentrate only on the most prominent effect (the moon) and ignore all others, an accurate model of the background brightness still requires a fair amount of complexity.

For now our background model simply adopts an empirical value for the continuum that remains constant in each band. For the $UBVRI$ bands these continuum values correspond to the broadband brightnesses as given by the standard ESO ETC sky brightness table for a moon phase of 3 days from new moon. These values are reproduced in Table 5.1. Any dependencies on the site and airmass are ignored.

In the near-IR the background brightness is dominated by the emission line component (mostly OH airglow) and hence the standard broadband sky brightnesses are inappropriate for the inter-line (pseudo-) continuum. Instead the model uses the continuum values measured with ISAAC by Cuby et al. (2000) in the J and H bands. The H-band value is also used in the K-band, beyond which the continuum is irrelevant. However, note that these values are highly uncertain and may depend on the details of the spectrograph. The true continuum may be significantly lower (e.g. Ellis & Bland-Hawthorn 2008). All continuum values are summarised in Table 5.1.

5.2 Emission lines

The emission lines (OH airglow) dominate the background in the near-IR, i.e. in the JHK bands. Although the airglow does not depend on moon phase it is known to vary systematically as a function of season

Table 5.1: Continuum brightness values.

Filter	Continuum brightness [γ/s/μm/m^2/arcsec^2]	[mag/arcsec^2]	Comment
U	190	21.5	Standard ESO ETC sky brightness
B	150	22.4	table for 3 days from new moon
V	210	21.7	
R_C	340	20.8	
I_C	500	19.9	
J	1200	18.0	Cuby et al. (2000)
H	2300	16.5	
K	2300	15.7	Extrapolation

and time of night, as well as randomly on shorter timescales and as a function of position on the sky. We have not attempted to model this and so the OH lines are always assumed to have the same strength. In particular, we have not (yet) included in the model any dependence of the OH airglow on the site or airmass.

[AD2] contains a compilation of optical and near-IR emission lines. The optical lines ($\lambda < 0.92$ μm) are from the UVES sky emission atlas (Hanuschik 2000; online data) while the near-IR lines are from the atlas of OH lines (Rousselot et al. 2000). The first column contains the line wavelength in μm and the second column contains the line flux (integrated over wavelength) in photons/s/m^2/arcsec^2.

5.3 Atmospheric emission

From the second half of the K-band onwards the background is dominated by the thermal emission from the atmosphere and the telescope. The atmospheric emission was calculated by A. Smette using the HITRAN molecular database and assuming a tropical atmospheric profile. Molecules included are: H_2O, CO, CO_2, CH_4, O_2, O_3 and N_2O. The calculations were performed for four different values of airmass and for each of the sites above.

[AD2] contains the atmospheric emission spectra for the various combinations of site, airmass and wavelength region (0.4–30 μm). The resolution of these spectra is 100 000.

5.4 Telescope emission

The emission from the telescope is modelled as a grey body (i.e. a black body multiplied by a constant emissivity ε). The telescope's emissivity is given in Section 6 and its temperature is that of the site's ambient temperature (see Section 4).

5.5 Discussion

The background model is shown in Figs. 5.1–5.3 at a resolution of R = 1000. The faint grey line in each of the figures shows a similar model from the Gemini exposure time calculator for Mauna Kea. The comparison highlights some of the uncertainties. The differences in the blue-optical are mainly due to different assumptions regarding the amount of the moonlight, although the Gemini model also rises quite steeply towards the red which is difficult to explain with just the moon. In the near-IR the model pseudo-continua are also different in shape (Fig. 5.2). The Gemini model assumes that the continuum is due to zodiacal light which is modelled by a grey body with a temperature of 5800 K and which is subject to atmospheric extinction. However, the normalisation is far too high for zodiacal light (by a factor of $\sim$70) and must be arbitrarily cut off near 0.9 μm in order to avoid producing far too much background light in the optical. The agreement in the OH lines, on the the other hand, is reasonable, and the apparent differences are mainly due to resolution. Note that the Gemini model does not include a telescope component. Hence

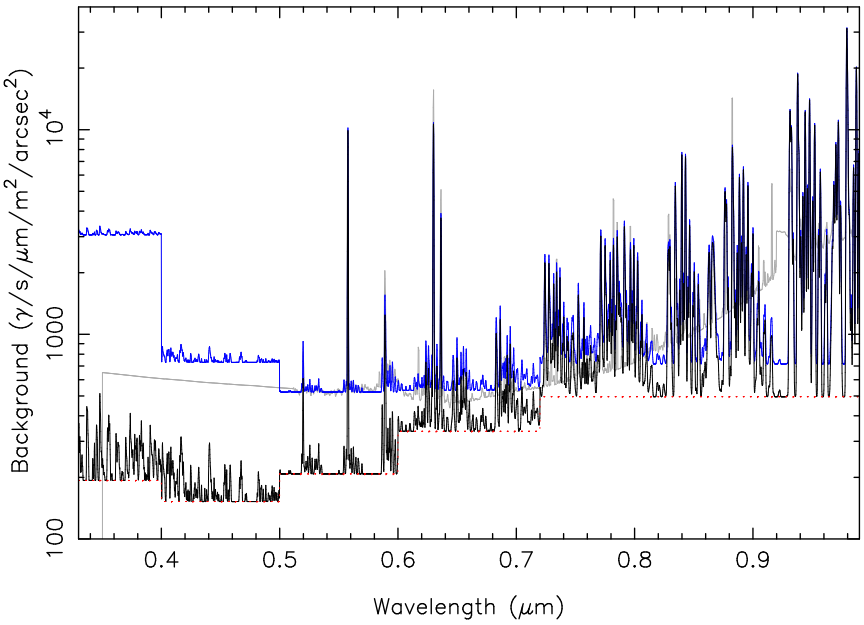

Figure 5.1: The black line shows the background model in the optical for 3 days from new moon and a resolution of R = 1000 (no site or airmass dependence). The dotted red line represents the continuum (which is assumed to be constant in each band). For comparison, the faint grey line shows an optical background model from the Gemini exposure time calculator for Mauna Kea and for a moon phase of 7 days from new moon. To match this model's photon flux in the V-band with our model we need to select a moon phase of 10 days from new moon, which is shown as the blue line.

the rise in the the second half of the K-band is solely due to the atmosphere. By comparing the two panels of Fig. 5.2 we can see that the model atmosphere for Mauna Kea lies in-between those for the Paranal-like site and the High & Dry site, as it should.

5.6 Atmospheric extinction

Atmospheric extinction is due to (at least) two different processes: molecular absorption and scattering by molecules and aerosols. The absorption is calculated by the same atmospheric model already described above, again for all combinations of airmass and site. Since scattering is only effective in the blue-optical, where molecular absorption is almost absent, we use a standard Paranal blue-optical extinction curve to represent the effect of scattering. The combined, total atmospheric transmission is hence given by

$$\xi(\lambda) = \xi_{\rm abs}(\lambda)\,\xi_{\rm sc}(\lambda) = \xi_{\rm abs}(\lambda)\,10^{-0.4\,\chi\,k(\lambda)} \tag{5.2}$$

where $\xi_{\rm abs}(\lambda)$ is given by the atmospheric model, χ is the airmass and $k(\lambda)$ is the extinction coefficient (= 0 for $\lambda > 0.7$ μm). For the High & Dry site the Paranal extinction curve is multiplied by 0.6 (Giraud et al. 2006). [AD2] contains the data files for $\xi_{\rm abs}(\lambda)$ and $k(\lambda)$, and the combined, total atmospheric transmission is shown in Figs. 5.4–5.6.

6 Telescope

6.1 Photon collecting area

The diameter of the telescope's primary mirror is	$D = 42$ m.
The diameter of the central obstruction is	$d = 0.28 \times D = 11.76$ m.
The photon collecting area is	$A = \pi/4\ (D^2 - d^2) = 0.92 \times \pi/4\ D^2 = 1276.82$ m^2.

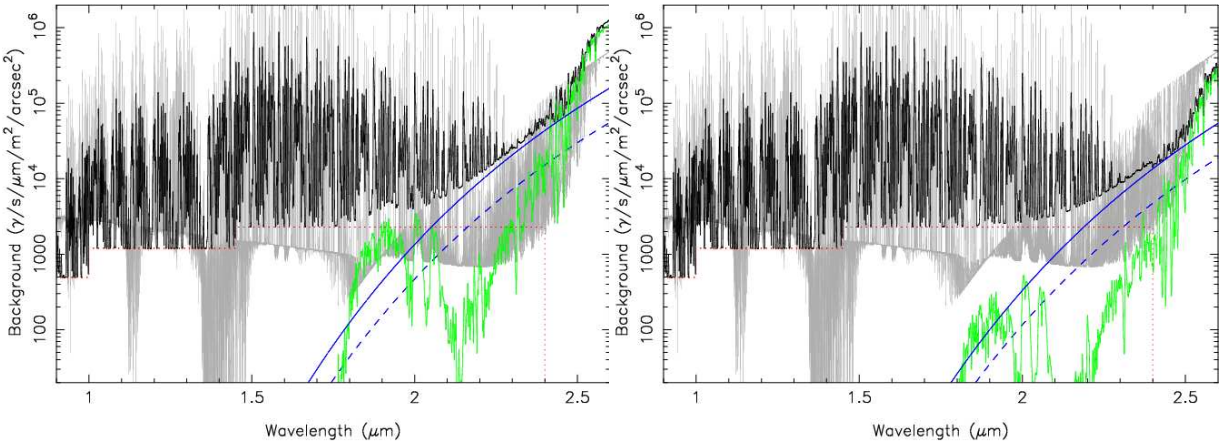

Figure 5.2: Left: The black line shows the background model in the near-IR for the Paranal-like site, 1 airmass, the bare aluminium coating (see Section 6) and a resolution of R = 1000. The dotted red line represents the continuum (which is assumed to be constant in each band but does not extend beyond the K-band). The blue (dashed) line represents the background from the telescope assuming the bare aluminium (protected silver/aluminium) coating, while the green line shows the thermal emission from the atmosphere. For comparison, the faint grey line shows a near-IR background model from the Gemini exposure time calculator for Mauna Kea (at a much higher resolution). Right: Same for the High & Dry site.

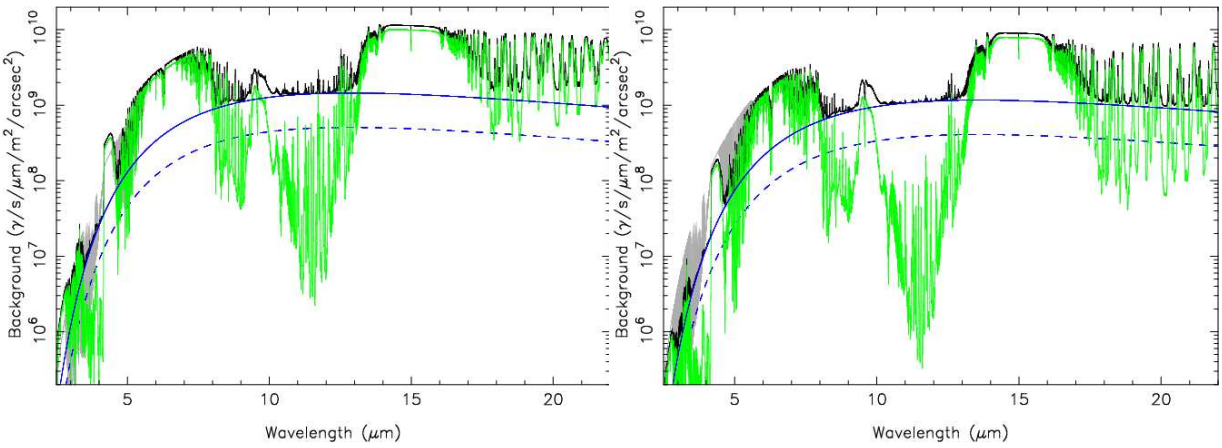

Figure 5.3: As Fig. 5.2 for the mid-IR. Note that the Gemini model (faint grey line) only extends to 5.6 μm.

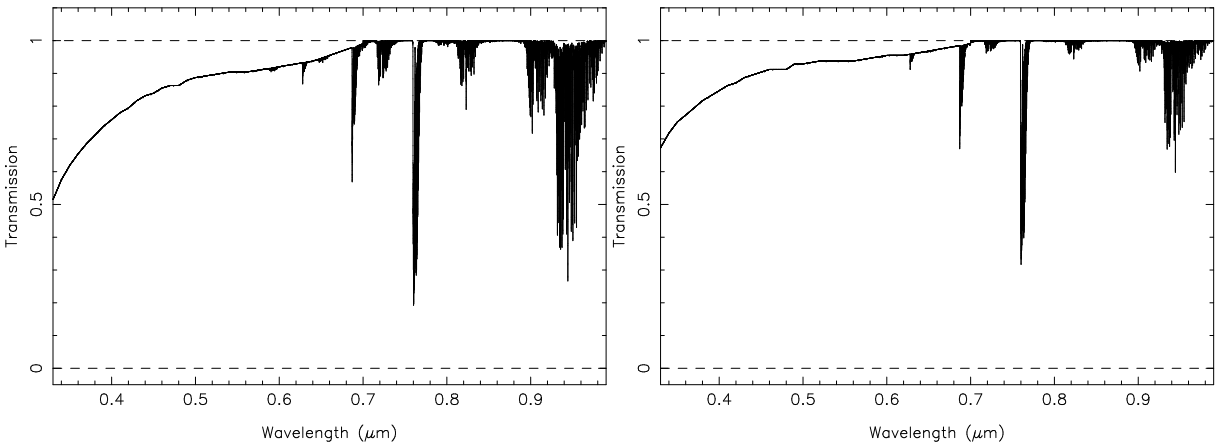

Figure 5.4: Left: The atmospheric transmission (extinction) in the optical for the Paranal-like site, 1 airmass and a resolution of R = 10 000. Right: Same for the High & Dry site.

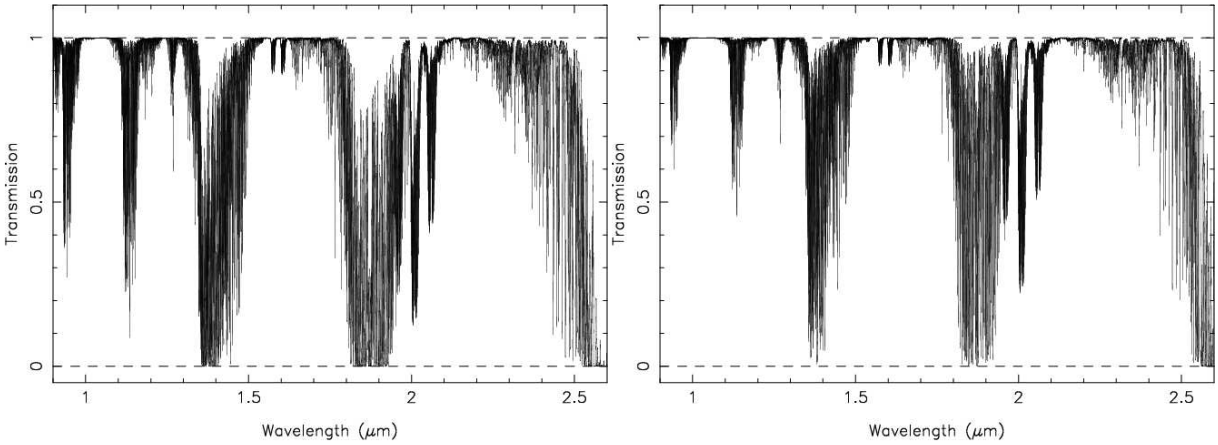

Figure 5.5: Same as Fig. 5.4 for the near-IR.

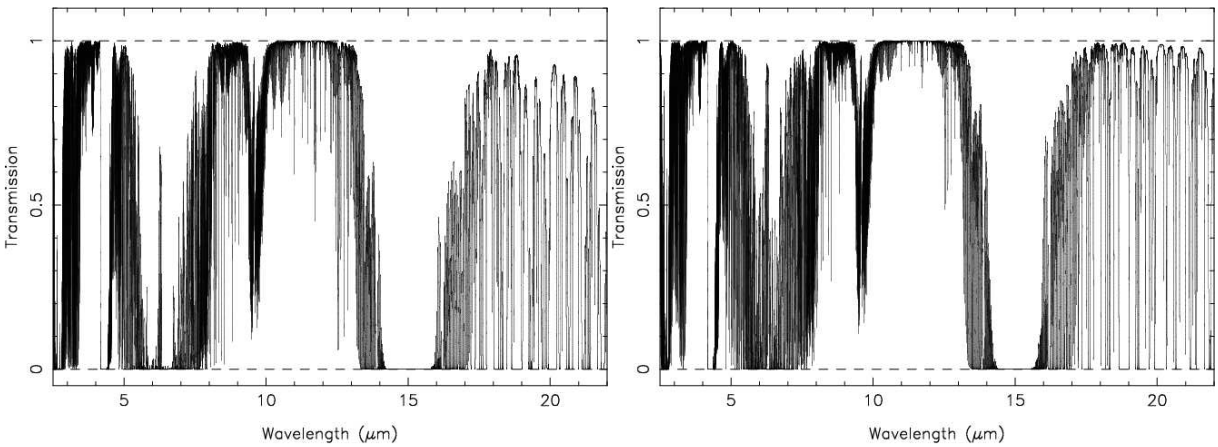

Figure 5.6: Same as Fig. 5.4 for the mid-IR.

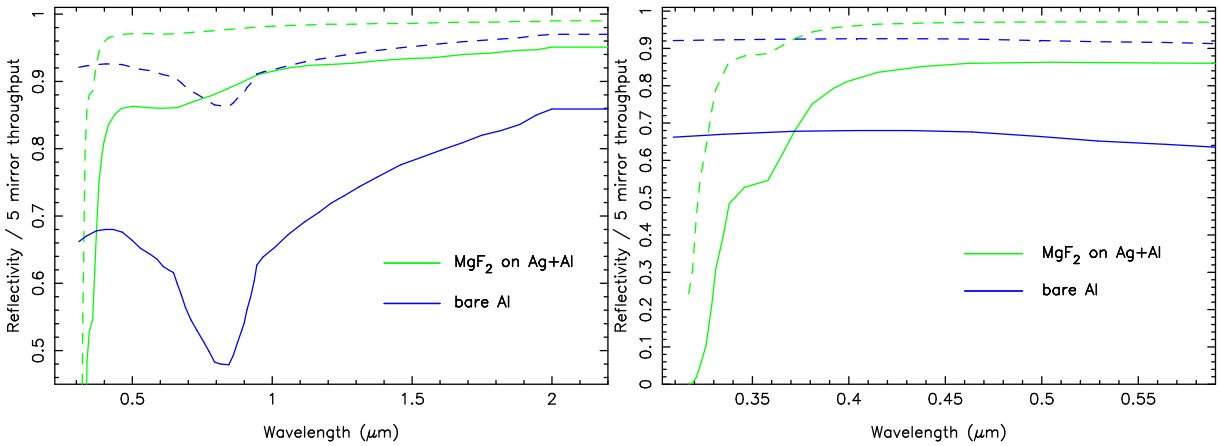

Figure 6.1: Left: The dashed green line shows the reflectivity for a protected silver/aluminium coating, while the dashed blue line shows the same for a bare aluminium coating. The solid lines show the respective throughputs after 5 mirrors. Right: Close-up of the UV-blue-optical region to highlight the dramatic difference between the two coatings in the UV.

The segmentation of the primary mirror and any obscuring support structures are ignored.

6.2 Throughput

The telescope is a 5-mirror design (i.e. 5 mirrors to the Nasmyth foci). The total throughput of the telescope (τ = ratio of the number of photons arriving at the Nasmyth foci to the number of photons impinging on the primary mirror) is hence the product of the reflectivities, R, of each of the 5 mirrors. It is assumed that all mirrors have the same reflectivity. Hence we have

$$\tau = R^5 \tag{6.1}$$

The reflectivity of a mirror is a function of wavelength and is determined by its coating. We consider two different coatings which have very dissimilar characteristics: the 'standard' bare aluminium coating and a more novel protected combination of silver and aluminium. Fig. 6.1 shows their reflectivities and total throughputs.

The protected silver/aluminium coating is clearly superior to the bare aluminium coating at all wavelengths $>$ 370 nm. In particular, aluminium shows the well-known dip near 800 nm, and the protected silver/aluminium coating retains a significant advantage all the way into the mid-IR (see below). However, only aluminium provides access to the UV down to the atmospheric cut-off.

[AD2] contains data files with the reflectivities and total throughputs.

These data were taken from the public TMT construction proposal. More information can be found in, e.g., Boccas (2004) who describes the first deployment of a protected silver coating at a large telescope (also summarised at this Gemini page).

6.3 Thermal emission

Each mirror is assumed to radiate like a grey body, i.e. its emission is given by $\varepsilon\, b(T)$, where $b(T)$ is a black body's emission, and ε and T are the mirror's emissivity and temperature, respectively. The temperature is assumed to be equal to that of the site. The emissivity of each mirror is given by $\varepsilon = 1 - R$, where R is the mirror's reflectivity at mid-IR wavelengths: $\varepsilon = 0.03$ for the bare aluminium coating and $\varepsilon = 0.01$ for the protected Ag/Al. Since all mirrors have the same temperature the total emission from the telescope

as seen by an instrument at the Nasmyth focus can be modelled as a single grey body with emissivity:

$$\varepsilon_{\rm tot} = \varepsilon \sum_{n=1\ldots5} (1-\varepsilon)^{n-1} = 1-(1-\varepsilon)^5 \approx 5\,\varepsilon\,(1-2\varepsilon) \tag{6.2}$$

Hence we obtain $\varepsilon_{\rm tot} = 0.14$ for the bare aluminium coating and $\varepsilon_{\rm tot} = 0.049$ for the protected Ag/Al coating.

Note that $\varepsilon_{\rm tot}$ is not simply equal to 5ε. The additional factor is due to the attenuation of a given mirror's radiation by the imperfect reflectivity of subsequent mirrors. For example, since the radiation emitted by the primary mirror has to be (imperfectly) reflected by the 4 subsequent mirrors in order to reach the focus, only a fraction R^4 actually makes it there.

7 Instruments

The available instruments and their parameters are not defined here. Rather, it is assumed that the instrumentation suite of the E-ELT is similar to the set of phase A instrumentation studies. In other words, each simulation should assume an instrument that is similar to one of the phase A concept studies. See [RD2] for an analysis of how the studied instruments relate to the DRM science cases.

7.1 Detectors

Table 7.1 lists the detector characteristics for the optical (U–I), near-IR (J–K) and mid-IR (L–Q) wavelength regions. Within each region all quantities are assumed to be constant as a function of wavelength.

Table 7.1: Detector characteristics.

	Optical	Near-IR	Mid-IR
Read-out noise	2 e^-	3 e^-	200 e^-
Dark current	2 e^-/h/pix	4 e^-/h/pix	2000 e^-/h/pix
Quantum efficiency	90 %	90 %	50 %

8 AO performance and PSFs

The performance of the adaptive optics (AO) is evaluated by simulating point spread functions (PSFs) using ESO's numerical AO simulation tool OCTOPUS. For each simulated PSF we also provide the parameters of an analytic fit to its radial intensity profile. This was obtained using `eltpsffit`, a custom-built tool to fit the numerically simulated PSFs with a combination of various analytical functions. The purpose of this tool is to obtain speckle-free, more manageable representations of the (very large) PSF images.

We also point out here that the MAORY consortium has also made its simulated MCAO PSFs available online.

8.1 PSF simulations

Here we give a basic description of ESO's numerical AO simulation tool OCTOPUS. Additional details are provided by Le Louarn et al. (2004, 2005).

The atmosphere is represented by a small number ($\approx$ 10) of infinitely thin turbulent layers which act as phase screens. Each screen is set up randomly and independently from one another according to a von Karman power spectrum of the refractive index fluctuations, i.e. a power-law spectrum with index $-11/3$ curtailed at finite inner and outer scales. The normalisation of each layer's power spectrum is given by

the atmosphere's C_n^2 profile, which describes the distribution of the turbulence in the atmosphere as a function oh height above the telescope.

The light from the (natural or laser) guide stars (NGS or LGS) is propagated to the wavefront sensors (WFS) using the geometrical optics approximation, i.e. tracking only phase fluctuations but not amplitude fluctuations (scintillation) of the light. The finite height of any LGS is taken into account by propagating their light in a conic fashion, rather than cylindrically as for real astronomical sources (like NGS). All WFS are assumed to be of the Shack-Hartmann type, i.e. an array of lenslets is used to produce multiple images of the guide star, each in its own sub-aperture on the WFS detector. The images on the WFS are formed by calculating the squared modulus of the Fourier transform of the incoming complex amplitude at the location of each lenslet. These images are then degraded by adding photon noise according to the guide star brightness and WFS integration time, as well as read-out noise. Subsequently, the centroids of the guide star images in all of the sub-apertures are measured, and all measurements from all WFS are assembled into a single vector. (Note that the calculation of the centroids ignores LGS spot elongation because new algorithms are currently being studied which will deal with this effect optimally.)

The position measurement vector is then multiplied with the AO system's pre-computed command matrix. The command matrix is the inverse of the interaction matrix which describes how the guide star positions in each of the WFS sub-apertures respond to a unit 'push' (or 'pull') from each of the deformable mirror's (DM) actuators. The result of multiplying the positional measurement vector with the command matrix is therefore a vector describing the positions of the DM's actuators that are required to compensate for the measured wavefront distortions. The DM is modelled as a special phase screen. Its shape (given by the actuators' positions and the assumed influence function) is subtracted from the phase of a wavefront coming in from the desired direction in the field of view (and propagated cylindrically). The resulting wavefront is then Fourier transformed to create a quasi-instantaneous or short exposure PSF, which is recorded.

To account for the temporal evolution of the atmosphere the above process is then repeated many times. Each iteration starts by shifting the phase screens representing the atmosphere by an amount determined by each layer's wind speed and the duration of one iteration in real time. Then the whole process of guide star wavefront propagation, wavefront sensing, DM shape calculation and short exposure PSF generation is repeated. Actually, the DM shape that is subtracted from the wavefront in any given iteration is not the shape computed in the same iteration, but rather the shape computed several iterations earlier. This delay accounts for the time required to integrate on the guide star (= 1 iteration), read-out the WFS detectors, compute the actuator positions, and actuate the DM.

Each iteration results in a short exposure PSF. All of these are summed together to generate the final, 'long' exposure PSF. However, since the frame rate of an AO system is typically 500–1000 Hz it takes thousands of iterations to cover just a few seconds of real time. Herein lies the main limitation of these simulations: since they are computationally so expensive it is impossible to generate truly long exposure PSFs (covering many minutes of real time) and one is limited to a few seconds of exposure time. The result is that residual speckles are still visible in the final PSFs which, of course, would not be present in real astronomical observations covering many minutes. This is obviously an undesirable feature when using these PSFs to simulate astronomical images. One way to overcome this limitation is to fit the simulated PSFs with a suitably chosen analytical function, or a combination of several different functions, in order to obtain a speckle-free representation.

Note that the above simulation process describes a *Monte Carlo* simulation: two realisations of the same PSF will differ from one another because of the random nature of the simulated atmosphere and because of the noise associated with the guide star images.

8.2 Simulation parameters

Obviously, there a large number of input parameters that are required for the simulations. Due to the computational cost of these simulations it is impossible to explore this parameter space comprehensively. Hence, only a relatively small number of input parameters (such as, e.g., the wavelength of observa-

tion) were varied to create different PSFs (see below). All other parameters were held constant for all simulations. These parameters and their values are listed in Table 8.1.

Table 8.1: PSF simulation parameters.

Atmosphere			
Fried parameter r_0	0.13 m at 0.5 μm		
Seeing	0.8 arcsec at 0.5 μm		
Turbulence power spectrum	von Karman		
Outer scale L_0	25 m		
Inner scale l_0	pixel size		
Number of turbulent layers	10		
Parameters of layers	Height [m]	Fractional C_n^2	Windspeed [m/s]
	0	0.335	12.1
	600	0.223	8.6
	1200	0.112	18.6
	2500	0.090	12.4
	5000	0.080	8.0
	9000	0.052	33.7
	11500	0.045	23.2
	12800	0.034	22.2
	14500	0.019	8.0
	18500	0.011	10.0
Laser guide stars	GLAO	LTAO	
Number of LGS	5	6	
LGS brightness	infinite	infinite	
LGS positions [arcmin from	$x = 3\cos(i \times 72°)$	$0.75\cos(i \times 72°), 0$	
field centre, $i = 0...4$]	$y = 3\sin(i \times 72°)$	$0.75\sin(i \times 72°), 0$	
Primary mirror			
Size and geometry	See Section 6.		
Wavefront sensors			
Number of WFS	equal to number of LGS		
Type	Shack-Hartmann		
Number of sub-apertures per WFS	84 $\times$ 84		
Number of CCD pixel per sub-aperture	6		
Noise	none (infinite flux, no read-out noise)		
Spot elongation	none		
Deformable mirrors			
Number of DMs	1		
Geometry	square		
Number of actuators per DM	85 $\times$ 85		
Actuator stroke	infinite		
Conjugation height	0 m		
Tile with respect to layers	none		
Influence function	linear spline		
Other parameters			
Frame rate	500 Hz		
Number of iterations	2000		
Total integration time	4 s		
Delay time	3 iterations		

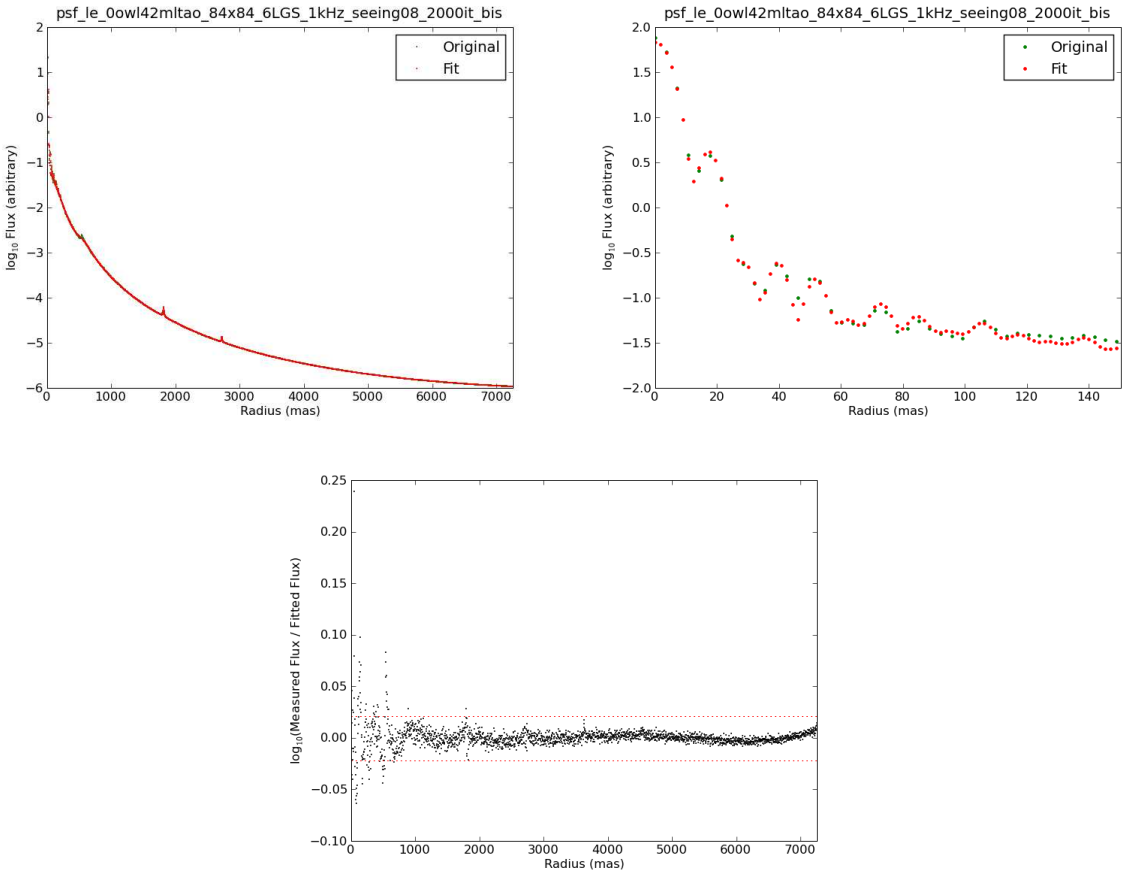

Figure 8.1: Example of a PSF fit with `eltpsffit`. Top left: The green points show the azimuthally averaged radial profile of a simulated LTAO, K-band, on-axis, 0° zenith distance PSF. The red points show the fit. Top right: zoom of the central region. Bottom: Residuals of the fit. The dashed red lines mark a deviation of the fit from the data of 5 %.

8.3 PSF fitting

In order to obtain speckle-free, more manageable representations of the PSF images, the radial profiles of all PSFs in the database have been fit with combinations of analytical functions using the custom-built tool `eltpsffit`. We only performed 1D fits of the PSF profiles, not 2D fits of the whole images, because generally full 2D fitting did not result in a significantly improved representation of the PSF.

High-Strehl PSFs were typically fit with four to five components: an (obstructed) Airy disk to represent the diffraction limited core and additional Lorentzian or Moffat function components to represent the halo. Low-Strehl PSFs usually required only two to three Lorentzian or Moffat components. Our (somewhat arbitrary) aim was to obtain fits that lie within 5 % of the data at all radii (not just in the centre). This was generally achieved except for the mid-IR LTAO PSFs which are much more difficult to fit. An example fit is shown in Fig. 8.1.

Note that these fits are not perfect representations of the PSFs. Different choices for the fitting weights, number or type of the fit components, etc., may well lead to more accurate descriptions, especially when considering only a restricted range of radii. Hence, depending on the application, one may wish to use `eltpsffit` to produce improved fits.

8.4 PSF database

All simulated PSF images (stored as fits files) are included in [AD2] in a directory tree structure, where the levels of the tree correspond to those input parameters that were varied to create different PSFs:

- type of AO
- zenith distance
- wavelength
- size of the field of view
- position within field of view

At a given level of the tree you will find one directory for each value of the level's corresponding parameter for which simulations were performed. The actual PSF images are contained in the lowest level directories. To find the PSF that corresponds to a particular combination of parameter values simply work your way down the directory tree.

Note that due to the computational cost of these simulations it is not possible to homogeneously populate even this relatively small 5-dimensional parameter space (let alone the full parameter space, see above). PSFs were generated only for those combinations of parameter values that have so far been deemed interesting or necessary. Hence some parts of parameter space are populated more densely than others, while other parts are entirely empty. Those combinations of parameter values that have so far not been simulated do not have corresponding branches in the database directory tree.

An existing branch usually only has one PSF image in its lowest level directory. However, for a few combinations of parameter values the simulations have been repeated, resulting in more than one realisation of the same PSF. In these cases the lowest level directory contains more than one PSF image. As explained above, all PSFs have been fitted with analytical functions in order to obtain a speckle-free representation. The files containing the results of the fits are also stored in the lowest level directories. These files have the same root filename as the corresponding PSF image but different extensions. At the top of each of these files we provide a brief description of their contents (see also these explanations).

Note that the fits header of each PSF image contains a record of the above parameter values that were used to simulate this PSF. The header also contains the usual basic image information such as the image's pixel size in mas (keywords CDELT1 and CDELT2).

The AO type 'NOAO' refers to the seeing-limited case (read: no AO). Zenith distance is given in degree. The wavelength of observation is given in m in the image headers, but is listed by the corresponding filter name in the database directory tree. The parameter 'size of the field of view' only applies to GLAO PSFs and is given in arcmin. This level is absent in the LTAO and NOAO parts of the directory tree. The parameter 'position within field of view' consists of an x and a y coordinate given in arcsec for LTAO and NOAO and in units of the size of the field of view for GLAO.

8.5 PSF properties

In Figs. 8.2–8.7 we show how the PSF behaves as a function of various parameters. Here we characterise the PSF in terms of its half-light radius, r_{50}, and the encircled energy within the diffraction limited core. Note that the latter quantity is really only useful when considering LTAO.

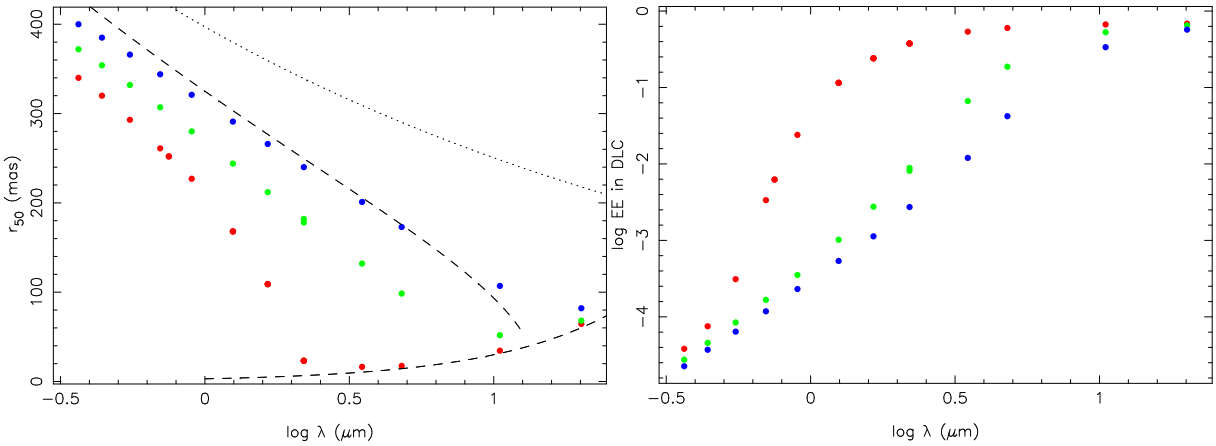

Figure 8.2: PSF as a function of wavelength. Blue = no AO, green = GLAO, red = LTAO. ZD = 0°, pos. in FoV = centre, GLAO: FoV = 6 arcmin. The dotted line in the left panel shows the wavelength dependence of r_{50} ($\propto \lambda^{-0.2}$) expected for an uncorrected PSF assuming an infinitely large outer scale of the atmospheric turbulence (L_0). Note that the blue no AO points are significantly offset towards lower values compared to this line, and that this offset increases towards longer wavelengths. The offset is due to the finite outer scale of the atmospheric turbulence that was assumed in the simulations. In the case of a D = 42 m telescope the aperture is in fact larger than the outer scale, so that the telescope 'sees' significantly less turbulence than it would if the outer scale were infinite, resulting in a pronounced reduction of the telescope seeing. The upper dashed line shows r_{50} after approximately correcting for this effect (using equation 20 of Tokovinin 2002). Both this curve and the dotted curve are normalised to the r_0 value used in the simulations. The lower dashed curve shows 0.5 $r_{\rm DLC}$, where $r_{\rm DLC} = 1.22\,\lambda/D$ is the radius of the diffraction limited core of a perfect PSF for a D = 42 m telescope. An ideal PSF will contain approximately half the flux within 0.5 $r_{\rm DLC}$ so that this radius is an approximate lower limit of r_{50}.

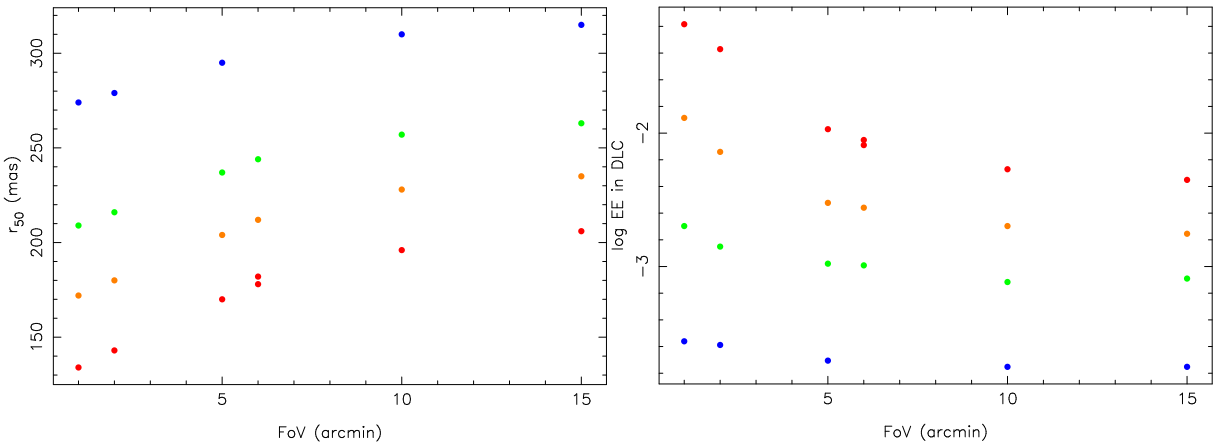

Figure 8.3: PSF as a function of the size of the field of view (GLAO only). Blue = I_C, green = J, orange = H, red = K. Type of AO = GLAO, ZD = 0°, pos. in FoV = centre. Note that there are two K-band PSFs at 6 arcmin (but none in the IC-band).

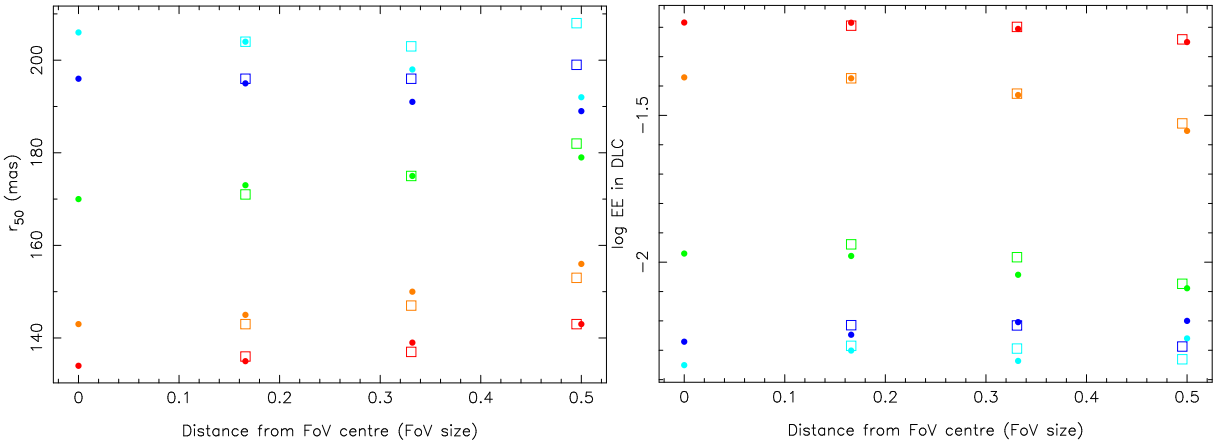

Figure 8.4: PSF as a function of position within the field of view (GLAO). Cyan = FoV of 15 arcmin, blue = 10, green = 5, orange = 2, red = 1. Type of AO = GLAO, ZD = 0°, $\lambda = K$. The distance from the centre of the field of view is given in units of the field's size. The solid dots refer to positions along the field-of-view's positive x-axis, while the open squares denote positions along a line that is inclined by 36° with respect to the x-axis. In the simulations the LGS were distributed in a ring around the field of view at 72° intervals, with one LGS lying on the positive x-axis. Hence, stepping along the solid dots one moves from the field's centre towards an LGS, whereas stepping along the open squares one moves from the centre outwards along a line bisecting two LGS. Note that this makes an appreciable difference for large field sizes.

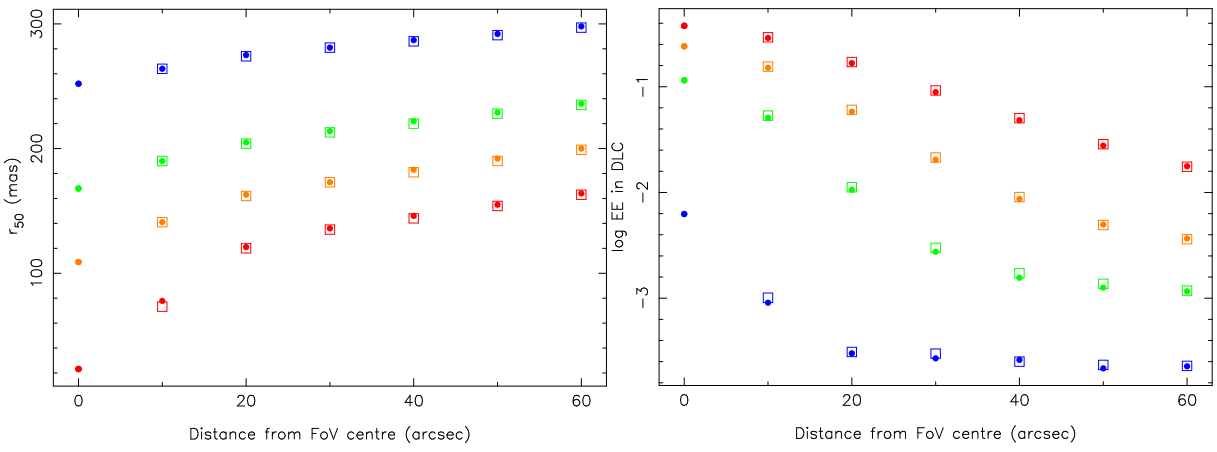

Figure 8.5: PSF as a function of position within the field of view (LTAO). Blue = I_C, green = J, orange = H, red = K. Type of AO = LTAO, ZD = 0°. The solid dots refer to positions along the field-of-view's positive x-axis, while the open squares denote positions along the field-of-view's positive y-axis. In the simulations the LGS were distributed in a ring around the field of view at 72° intervals, with one LGS lying on the positive x-axis. Hence, stepping along the solid dots one moves from the field's centre towards an LGS, whereas stepping along the open squares one moves from the centre outwards along a line that is one quarter between the second and third LGS.

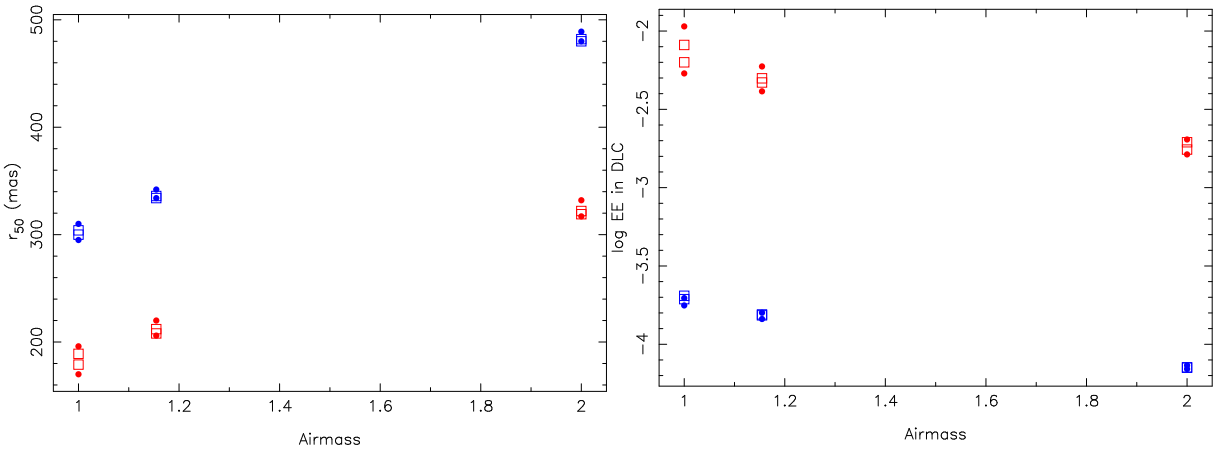

Figure 8.6: PSF as a function of airmass (GLAO). Blue = I_C, red = K. Solid dots = pos. in FoV: centre, open squares = 0.5, 0. Type of AO = GLAO, FoV = 5 and 10 arcmin (lower and upper points on left panel; vice versa on right panel). The shown airmasses correspond to zenith distances of 0°, 30° and 60°.

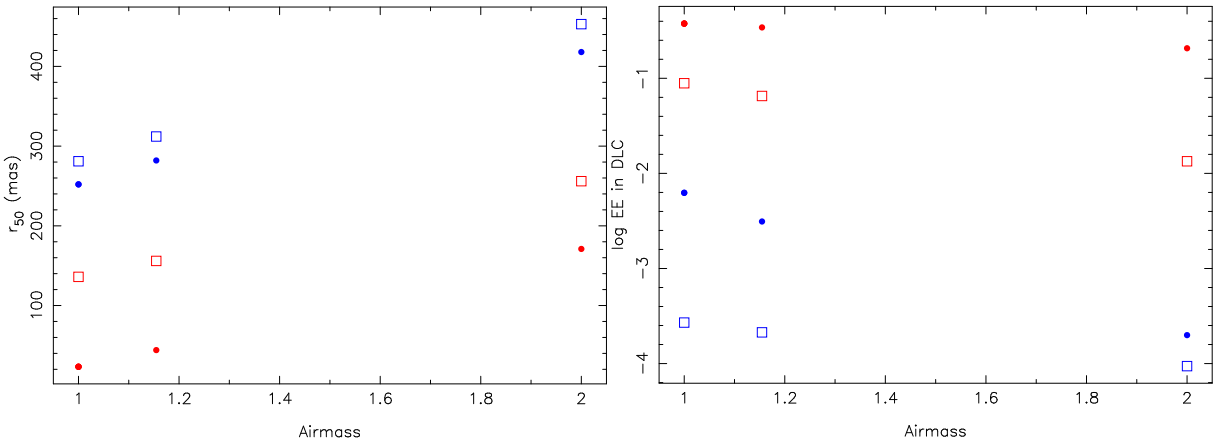

Figure 8.7: PSF as a function of airmass (LTAO). Blue = I_C, red = K. Solid dots = pos. in FoV: centre, open squares = 30, 0 arcsec. Type of AO = LTAO. The shown airmasses correspond to zenith distances of 0°, 30° and 60°.

9 Photometric system definitions

Table 9.1 lists the central wavelengths, widths and zero-points for a variety of filters. [AD2] includes this table as a data file which also contains the zero-points in additional units. [AD2] also contains data files with the individual filter curves. These have been arbitrarily normalised to a unity peak value. Several of these filter curves are shown in Fig. 9.1.

Table 9.1: Photometric system definitions.

Filter	λ_c [μm]	FWHM [μm]	$2.5 \log f^a_{\lambda 0}$ [erg/s/cm^2/Å]		$2.5 \log f^a_{\nu 0}$ [erg/s/cm^2/Hz]		$N^b_{\rm phot}$ [γ/s/cm^2/Å]	
			Vega	AB	Vega	AB	Vega	AB
U	0.366	0.065	-20.95	-20.23	-49.32	-48.60	7.69e+02	1.50e+03
B	0.436	0.089	-20.50	-20.62	-48.48	-48.60	1.39e+03	1.25e+03
V	0.545	0.084	-21.10	-21.09	-48.61	-48.60	9.96e+02	1.01e+03
R_C	0.641	0.160	-21.66	-21.44	-48.81	-48.60	7.02e+02	8.55e+02
I_C	0.798	0.150	-22.37	-21.92	-49.05	-48.60	4.52e+02	6.87e+02
J	1.22	0.213	-23.76	-22.84	-49.52	-48.60	1.93e+02	4.49e+02
H	1.63	0.307	-24.86	-23.47	-49.99	-48.60	9.34e+01	3.36e+02
K_s	2.12	0.32	-25.87	-24.04	-50.43	-48.60	4.78e+01	2.58e+02
K	2.19	0.39	-26.01	-24.11	-50.50	-48.60	4.37e+01	2.50e+02
L	3.45	0.472	-27.87	-25.10	-51.38	-48.60	1.23e+01	1.59e+02
L'	3.80	0.65	-28.28	-25.31	-51.57	-48.60	9.35e+00	1.44e+02
R	0.7	0.22	-21.89	-21.63	-48.86	-48.60	6.17e+02	7.83e+02
I	0.88	0.24	-22.69	-22.13	-49.16	-48.60	3.72e+02	6.23e+02
M	4.769	0.45	-29.19	-25.80	-51.99	-48.60	5.06e+00	1.15e+02
N	10.472	5.19	-32.54	-27.51	-53.63	-48.60	5.08e-01	5.23e+01
Q	20.130	7.8	-35.36	-28.93	-55.03	-48.60	7.28e-02	2.72e+01
u	0.355	0.064	-	-20.12	-	-48.56	-	1.60e+03
g	0.467	0.135	-	-20.75	-	-48.60	-	1.17e+03
r	0.617	0.137	-	-21.36	-	-48.60	-	8.88e+02
i	0.748	0.154	-	-21.78	-	-48.60	-	7.33e+02
z	0.893	0.147	-	-22.18	-	-48.62	-	6.02e+02

[a] $f_{\lambda 0}$ and $f_{\nu 0}$ refer to the flux at 0 mag.
[b] Number of photons at 0 mag.
References: U–L': Bessel et al. (1998); RI: Cox (2000); MNQ: Cohen et al. (1992); u–z: SDSS; AB zero-point: Oke (1974).

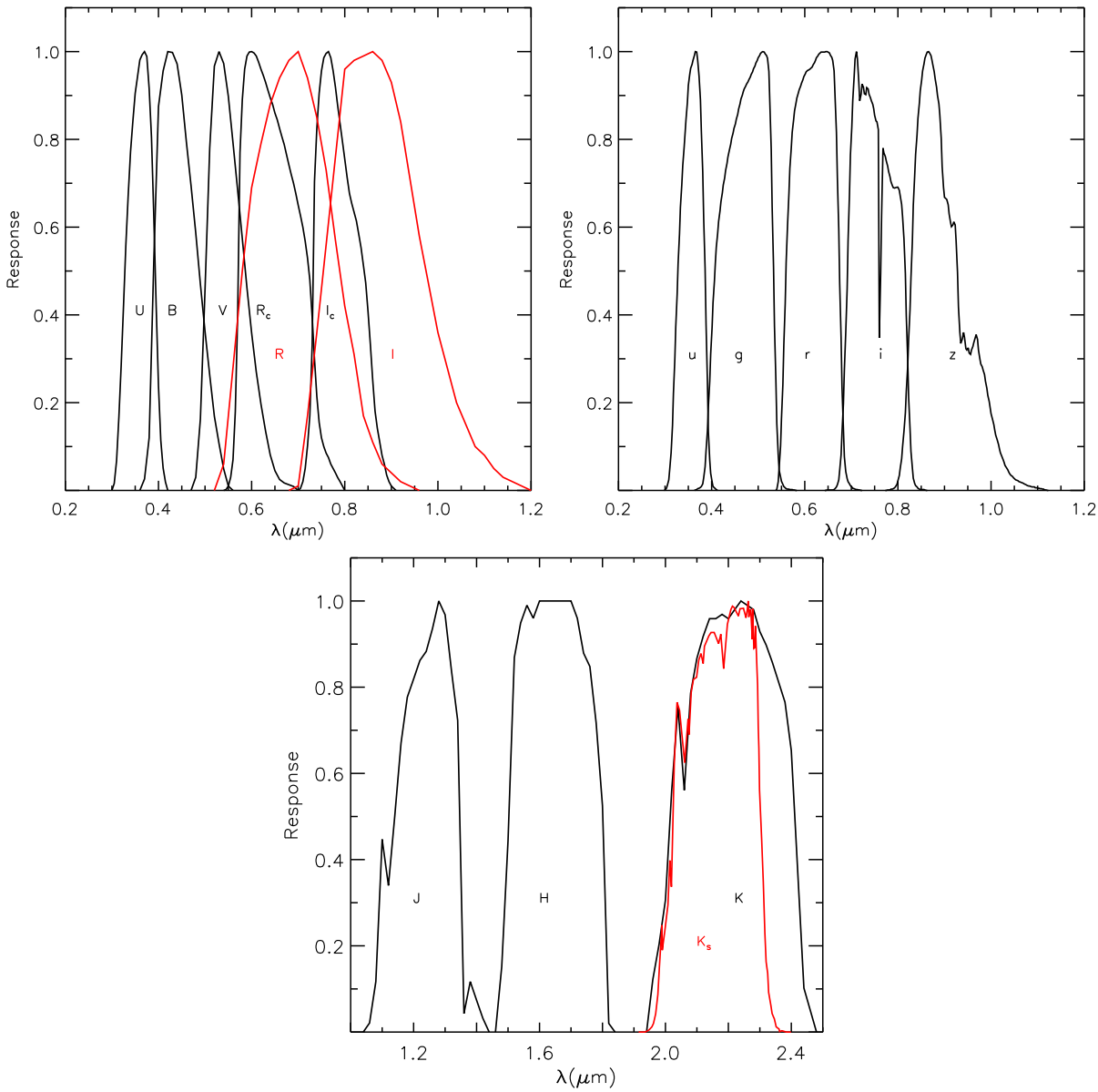

Figure 9.1: Selection of filter curves for popular bands.

10 The E-ELT imaging ETC

In this section we provide a description of the E-ELT imaging ETC (version 2.14). The S/N calculation performed by this ETC depends on a large number of parameters. To separate those parameters that are user inputs from those that are fixed, we use green text to mark the user input parameters (and the available options for the parameter where applicable).

10.1 Definitions

This section defines all parameters, symbols, terms, units and formulae needed for the S/N calculation. More detailed explanations follow in Section 10.2.

- $m_{\rm obj}$: Object magnitude (for a point source or extended source) or object surface brightness in a specified band (options: U–Q) and magnitude system (Vega or AB). [mag or mag/arcsec^2]
- r_h: Half-light radius for use with an extended source. [mas]
- $F_0 \equiv 10^{-Z}$: Photometric zeropoint. [W/m^2/μm]
  May be either Vega or AB. The various values for the different bands are listed in Table 9.1.
- $F_{\rm obj}$: Object flux (point source or extended source) or surface brightness at the top of the atmosphere. [W/m^2/μm or W/m^2/μm/arcsec^2]
  $F_{\rm obj} = F_0 10^{-0.4\ m_{\rm obj}}$.
  Instead of $m_{\rm obj}$ the user can also directly specify $F_{\rm obj}$ [mJy or mJy/arcsec^2].
- Observatory site: Paranal-like or High & Dry.
  The choice of site affects the atmospheric extinction as well as the sky surface brightness in the mid-IR (but not in the optical or near-IR). Site parameters are listed in Table 4.1.
- χ: Airmass.
  Affects the atmospheric extinction (but not the sky surface brightness).
- D: Telescope diameter. [m]
  Options: 8.2, 30 or 42 m. Note that changing this parameter only affects the size of the photon collecting area but *not* the PSF.
- A: Photon collecting area of the telescope. [m^2]
  $A = \frac{\pi}{4}(D^2 - d^2)$, where d is the diameter of the central obstruction. We assume $d = 0.28\,D$, i.e. that the central obstruction reduces the unobscured collecting area by 8%.
- AO mode: Seeing limited (i.e. no AO), Ground Layer AO (GLAO) or Laser Tomography AO (LTAO). Affects the PSF.
- λ_c: Central wavelength of the chosen observing band. [μm]
- p: Pixel scale. [mas/pixel]
  Options: 5, 10, 50 or 100 mas.
- Ω_p: Sky aperture per pixel. [mas^2/pixel]
  $\Omega_p = p^2$.
- $N_{\rm pix}$: Number of pixel in the S/N reference area.
  For a point source, $N_{\rm pix}$ is an input parameter. Options: 1×1, 3×3, 5×5 or 10×10 pixel.
  For an extended source or a constant surface brightness: $N_{\rm pix} = \Omega/(10^{-6}\ \Omega_p)$.

- Ω: Size of the S/N reference area. [arcsec^2]

  For a point source: $\Omega = 10^{-6}\ N_{\rm pix}\ \Omega_p$.
  For an extended source: $\Omega = 10^{-6}\ \pi\ {r_h}^2$.
  For a constant surface brightness: $\Omega = 1$ arcsec^2.

- $\Delta\lambda$: Wavelength range that is used for the integration over wavelength. [μm]

  The various values for the different bands are listed in Table 9.1. $\Delta\lambda$ is equivalent to an effective filter width.

- ξ: Atmospheric extinction.

  Depends on site, airmass and the chosen observing band. $\xi = 10^{-0.4\ \chi\ k}$, where k is the extinction coefficient for the chosen site and observing band. The various coefficients are given in [AD2] (see Section 5.6). Note: for now we only consider extinction due to scattering but neglect the atmospheric absorption at IR wavelengths.

- $\hat{F}_{\rm obj}$: Object flux (point source or extended source) or object surface brightness at the telescope entrance. [W/m^2/μm or W/m^2/μm/arcsec^2]

  $\hat{F}_{\rm obj} = \xi F_{\rm obj}$.

- ϵ: Total efficiency.

  Set to 0.5. This is the ratio between the number of detected photo-electrons and the number of photons incident at the telescope entrance, i.e. it includes the telescope, instrument and detector, but excludes the atmosphere.

- E_γ: Photon energy at λ_c. [J/γ]

  $E_\gamma = 1.985 \times 10^{-19}/\lambda_c$.

- c: Total conversion factor from energy flux incident at the telescope entrance to detected number of photo-electrons. [e$^-$/s per W/m^2/μm]

  $c = \epsilon\ \Delta\lambda\ A/E_\gamma$.

- T: Detector exposure time for one exposure (DIT). [s]

- $n_{\rm exp}$: Number of exposures (NDIT).

- e: Ensquared energy or fraction of PSF in the S/N reference area.

  For a point source this value is looked up in Table 10.3, 10.4 or 10.5 as appropriate for the chosen AO mode, using the observing band and the linear size of the S/N reference area as input.
  For an extended source: $e = 0.5$.
  For a constant surface brightness this parameter is not needed.

- $N_{\rm obj}$: Number of detected electrons from object in the S/N reference area per exposure. [e$^-$]

  For a point source or an extended source: $N_{\rm obj} = \hat{F}_{\rm obj}\ e\ c\ T$.
  For a constant surface brightness: $N_{\rm obj} = \hat{F}_{\rm obj}\ \Omega\ c\ T$.

- $m_{\rm sky}$: Sky surface brightness in selected observing band. [mag/arcsec^2]

  The various values for the different bands are listed in Table 10.1.

- $F_{\rm sky}$: Sky surface brightness at the top of the atmosphere. [W/m^2/μm/arcsec^2]

  $F_{\rm sky} = F_0 10^{-0.4\ m_{\rm sky}}$.

- $\hat{F}_{\rm sky}$: Sky surface brightness at the telescope entrance. [W/m^2/μm/arcsec^2]

  $\hat{F}_{\rm sky} = \xi F_{\rm sky}$.

- $N_{\rm sky}$: Number of detected electrons from the background in the S/N reference area per exposure. [e$^-$]

  $N_{\rm sky} = \hat{F}_{\rm sky}\ \Omega\ c\ T$.

- d: Detector dark current. [e$^-$/s/pixel]
  See Table 7.1.
- r: Detector read-out noise. [e$^-$/pixel]
  See Table 7.1.
- S/N: Signal-to-noise ratio.

$$S/N = \frac{\sqrt{n_{\rm exp}}\, N_{\rm obj}}{\sqrt{N_{\rm obj} + N_{\rm sky} + N_{\rm pix}\, r^2 + N_{\rm pix}\, d\, T}}.$$

10.2 Explanations

10.2.1 The target

The target's flux is specified by giving its magnitude in any one of the allowed bands (U to Q), and its flux distribution. The zero-points of the magnitude scale may be either Vega or AB (cf. Table 9.1). The flux distribution determines a colour term which is applied to the input magnitude in case the band in which the object's magnitude is specified differs from the observation band (which can also be chosen from U to Q). Unfortunately, no such colour terms are currently available for the N and Q bands. That means that the ETC will only work for these bands when the band of the target's magnitude and the observation band are both set to the same value. Alternatively, the target's flux at the central wavelength of the observation band may be specified directly in mJy.

The source geometry can be chosen to be a point source, an extended source or a constant surface brightness value. For an extended source the user must also specify its half-light radius, r_h, which is assumed to include the effects of the PSF (as chosen by the user, see below). Thus, a warning will be issued if the user specifies an r_h smaller than the half-light radius of the PSF of the chosen AO mode. The values for these minimum r_h values are listed in Table 10.2 and shown in Fig. 8.2 (left panel). For the case of constant surface brightness the target magnitude is assumed to denote a surface brightness in mag/arcsec^2.

10.2.2 The S/N reference area

The S/N calculation is performed using the light collected in the 'S/N reference area'. For an extended source the ETC assumes that the light from the object (and the sky) is collected over an area πr_h^2, and that this area contains half of the object's total light as given by the user-specified target magnitude. For a constant surface brightness the light from the object (and sky) is collected over a fixed 1 arcsec^2. For a point source the user can choose the size of the S/N reference area as either 1×1, 3×3, 5×5 or 10×10 pixel. The size of the S/N reference area on the sky is of course further affected by the user's choice of the pixel scale.

The fraction of a point source's flux within a given S/N reference area is determined by the chosen AO mode: Seeing limited (i.e. no AO), Ground Layer AO, or Laser Tomography AO. For a given AO mode and observing band the fractional energy ensquared by the S/N reference area is obtained from a look-up table. The tables for the various AO modes are reproduced in Tables 10.3, 10.4 and 10.5, and are presented graphically in Figs. 10.1, 10.2 and 10.3. The values in these tables were measured from simulated PSFs described in Section 8. All PSF simulations assume a DIMM seeing of FWHM = 0.8 arcsec at 0.5 μm and a 42 m telescope. Note that we do not have simulations for an 8.2 or 30 m telescope, which can also be chosen by the user. Hence, making these choices for the diameter affects only the photon collecting area, but *not* the PSF. Similarly, the PSFs do not change when selecting different sites or airmasses. Finally, we note that the E-ELT is likely to offer AO modes other than those listed above, such as Multi-Conjugate AO or Extreme AO. Currently, we lack appropriate PSF simulations to properly include these AO modes in the ETC. However, in the case of MCAO it is probably not too unreasonable to assume similar performance as for LTAO.

Table 10.1: Sky brightness values (for 3 days from new moon). These values were derived from the model described in Section 5.

Band	Paranal-like $m_{\rm sky}$ [mag/arcsec^2]	High & Dry $m_{\rm sky}$ [mag/arcsec^2]
U	21.5	21.5
B	22.4	22.4
V	21.7	21.7
R	20.8	20.8
I	19.9	19.9
J	16.0	16.0
H	14.0	14.0
K	13.0	13.0
L	5.3	6.2
M	1.3	2.3
N	-3.7	-3.2
Q	-6.5	-5.8

The site only affects the sky brightness at mid-IR wavelengths. Any site dependence at optical and near-IR wavelengths is ignored. Any airmass dependence is also ignored (at all wavelengths). The sky brightness values are given in Vega mags.

Table 10.2: Minimum r_h.

Filter	$r_{h,\rm min}$ [arcsec]		
	No AO	GLAO	LTAO
U	0.400	0.371	0.340
B	0.385	0.354	0.320
V	0.365	0.332	0.292
R	0.344	0.307	0.262
I	0.321	0.280	0.227
J	0.291	0.243	0.169
H	0.267	0.211	0.109
K	0.240	0.177	0.023
L	0.201	0.132	0.017
M	0.173	0.099	0.018
N	0.107	0.052	0.035
Q	0.082	0.068	0.065

$r_{h,\rm min}$ is the smallest allowed half-light radius for extended objects. It is defined as the 50% encircled energy radius of the PSF (for a D=42 m telescope).

Table 10.3: Ensquared energies for seeing limited case (no AO). These values were derived from the PSF simulations described in Section 8.

Linear size of S/N ref. area	Percentage of energy enclosed in the S/N reference area											
[mas]	U	B	V	R	I	J	H	K	L	M	N	Q
5	0.00379	0.00427	0.00465	0.00538	0.00627	0.00784	0.00775	0.0105	0.0241	0.0600	0.263	0.143
10	0.0152	0.0168	0.0185	0.0216	0.0251	0.0309	0.0330	0.0448	0.0970	0.238	1.05	0.570
15	0.0345	0.0377	0.0415	0.0483	0.0571	0.0689	0.0796	0.108	0.210	0.504	2.32	1.28
25	0.0958	0.104	0.116	0.136	0.157	0.198	0.241	0.313	0.565	1.32	5.69	3.57
30	0.138	0.149	0.167	0.194	0.227	0.287	0.347	0.454	0.793	1.79	7.59	5.09
50	0.383	0.418	0.465	0.534	0.625	0.777	0.964	1.21	2.12	4.14	18.2	11.8
100	1.52	1.66	1.86	2.12	2.46	3.07	3.68	4.78	7.86	11.8	32.2	37.5
150	3.36	3.67	4.11	4.68	5.42	6.66	8.04	10.1	15.4	21.7	41.6	51.2
250	8.98	9.76	10.8	12.3	14.0	16.9	20.0	24.0	32.9	40.1	58.2	60.8
300	12.6	13.6	15.1	17.0	19.3	23.0	26.9	31.7	41.1	48.4	63.2	67.0
500	30.2	32.2	34.9	38.2	42.1	47.6	52.6	58.0	66.1	70.7	78.6	80.6
1000	70.5	72.2	74.4	76.9	79.4	82.4	84.6	86.5	88.8	90.0	91.4	90.9

Table 10.4: Ensquared energies for GLAO. These values were derived from the PSF simulations described in Section 8.

Linear size of S/N ref. area	Percentage of energy enclosed in the S/N reference area											
[mas]	U	B	V	R	I	J	H	K	L	M	N	Q
5	0.00460	0.00524	0.00613	0.00752	0.00974	0.0155	0.0220	0.0495	0.378	0.738	0.499	0.171
10	0.0184	0.0208	0.0243	0.0300	0.0384	0.0592	0.0884	0.188	1.25	2.60	2.00	0.683
15	0.0413	0.0465	0.0550	0.0659	0.0866	0.129	0.199	0.397	2.52	5.04	4.42	1.54
25	0.115	0.128	0.149	0.186	0.233	0.347	0.553	1.02	4.58	11.5	10.5	4.27
30	0.166	0.185	0.217	0.266	0.336	0.497	0.782	1.43	5.50	13.2	14.2	6.19
50	0.458	0.513	0.602	0.732	0.915	1.36	2.06	3.66	9.85	18.5	34.0	14.1
100	1.81	2.03	2.38	2.87	3.59	5.12	7.36	11.4	22.8	34.6	51.9	44.9
150	4.01	4.49	5.21	6.23	7.74	10.7	14.9	21.1	34.0	45.2	61.1	59.6
250	10.6	11.7	13.4	15.8	19.0	24.9	31.4	39.8	52.1	60.3	74.9	68.6
300	14.7	16.3	18.5	21.5	25.4	32.2	39.3	47.6	59.0	66.0	77.5	74.7
500	34.1	36.8	40.4	44.8	49.8	56.8	62.7	68.5	75.9	79.9	85.7	86.0
1000	73.7	75.4	77.6	79.9	82.1	84.7	86.6	88.3	90.3	91.5	93.2	92.7

Table 10.5: Ensquared energies for LTAO. These values were derived from the PSF simulations described in Section 8.

Linear size of S/N ref. area	Percentage of energy enclosed in the S/N reference area											
[mas]	U	B	V	R	I	J	H	K	L	M	N	Q
5	0.00641	0.00850	0.0239	0.218	1.34	4.65	6.48	6.60	4.55	2.75	0.648	0.182
10	0.0254	0.0338	0.0752	0.451	2.46	10.2	17.4	21.5	14.5	9.72	2.59	0.727
15	0.0569	0.0748	0.148	0.676	3.39	12.2	23.0	31.2	28.8	18.9	5.83	1.64
25	0.156	0.201	0.353	1.10	4.48	16.5	29.1	38.4	47.3	42.4	13.7	4.54
30	0.224	0.285	0.482	1.33	4.86	17.4	32.3	42.2	52.3	48.1	18.2	6.54
50	0.619	0.774	1.19	2.49	6.58	19.6	35.5	51.6	60.7	60.0	44.8	15.1
100	2.42	2.96	4.15	6.86	12.5	25.1	40.3	55.9	72.5	78.8	66.2	47.8
150	5.31	6.37	8.44	12.4	19.2	32.3	45.0	59.0	75.5	80.6	75.0	63.2
250	13.5	15.7	19.4	24.8	32.4	44.7	55.3	65.6	78.8	84.4	87.1	72.0
300	18.4	21.2	25.3	31.2	38.5	49.9	59.5	68.6	79.9	85.3	87.9	78.4
500	39.5	43.0	47.7	53.0	58.6	65.4	71.3	77.3	84.7	88.3	91.7	89.0
1000	75.9	77.3	79.0	80.9	82.8	85.0	86.6	88.0	90.7	92.5	94.6	93.8

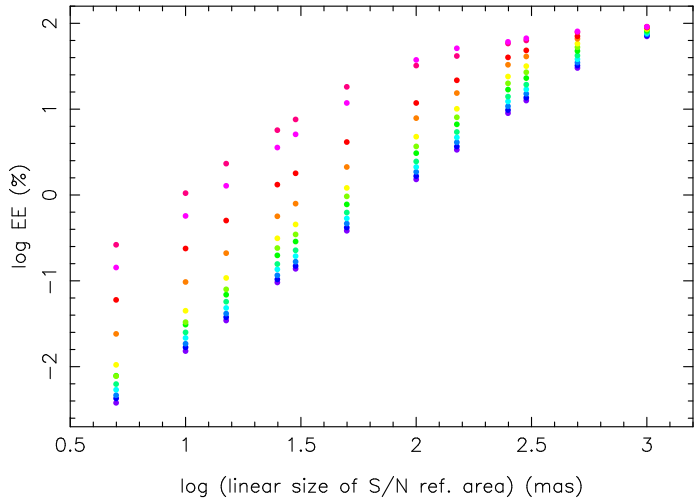

Figure 10.1: Ensquared energy as a function of the linear size of the S/N reference area for no AO, i.e. a graphical representation of Table 10.3. Different bands are represented by differently coloured points.

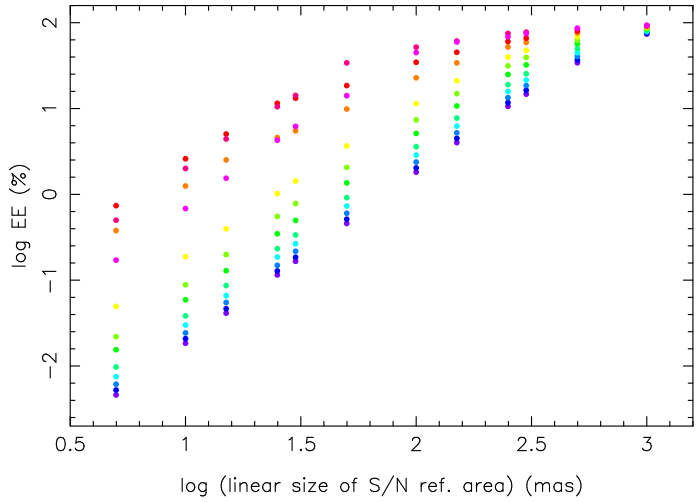

Figure 10.2: Ensquared energy as a function of the linear size of the S/N reference area for GLAO, i.e. a graphical representation of Table 10.4. Different bands are represented by differently coloured points.

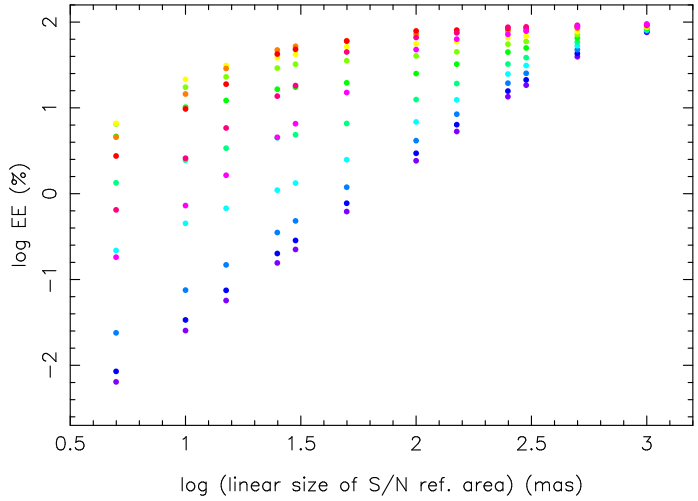

Figure 10.3: Ensquared energy as a function of the linear size of the S/N reference area for LTAO, i.e. a graphical representation of Table 10.5. Different bands are represented by differently coloured points.

11 The E-ELT spectroscopic ETC

In this section we provide a description of the E-ELT spectroscopic ETC (version 2.14). As in the previous section we use green text to mark the user input parameters (and the available options for the parameter where applicable).

11.1 Definitions

This section defines all parameters, symbols, terms, units and formulae needed for the S/N calculation. More detailed explanations follow in Section 11.2.

- $m_{\rm obj}$: Object magnitude (for a point source) or object surface brightness (for an extended source) in a specified band (options: U–Q) and magnitude system (Vega or AB). [mag or mag/arcsec^2]
- $F_0 \equiv 10^{-Z}$: Photometric zeropoint. [W/m^2/μm]

  May be either Vega or AB. The various values for the different bands are listed in Table 9.1.
- $F_{\rm obj}$: Object flux (point source) or surface brightness (extended source) at the top of the atmosphere. [W/m^2/μm or W/m^2/μm/arcsec^2]

  $F_{\rm obj} = F_0 10^{-0.4\ m_{\rm obj}}$.

  This formula is only strictly true for the case of a uniform flux distribution. Otherwise $m_{\rm obj}$ is used to normalise the flux distribution so that the distribution's integral over the band is equal to the flux given by $m_{\rm obj}$. Instead of $m_{\rm obj}$ the user can also directly specify $F_{\rm obj}$ [mJy or mJy/arcsec^2].
- Observatory site: Paranal-like or High and Dry.

  The choice of site affects the atmospheric emission (only at mid-IR wavelengths) and transmission. Site parameters are listed in Table 4.1.
- χ: Airmass.

  Options: $1,\ 1.15,\ 1.5$ or 2. Affects the atmospheric emission (only at mid-IR wavelengths) and transmission.
- D: Telescope diameter. [m]

  Options: $8.2,\ 30$ or 42 m. Note that changing this parameter only affects the size of the photon collecting area but *not* the PSF.
- A: Photon collecting area of the telescope. [m^2]

  $A = \frac{\pi}{4}(D^2 - d^2)$, where d is the diameter of the central obstruction. We assume $d = 0.28\,D$, i.e. that the central obstruction reduces the unobscured collecting area by 8%.
- AO mode: Seeing limited (i.e. no AO), Ground Layer AO (GLAO) or Laser Tomography AO (LTAO). Affects the PSF.
- $R_{\rm ref}$: Radius of the circular S/N reference area. [mas]

  Options: various values in the range 2.2–1000 mas.
- Ω: Size of the S/N reference area. [arcsec^2]

  $\Omega = \pi R_{\rm ref}^2 / 10^6$.
- $N_{\rm spec}$: Number of individual spectra on the detector over which the light from the S/N reference area is spread. This may be equal to the number of separate spatial elements (spaxel) in the S/N reference area.
- $\lambda_{\rm ref}$: Observing wavelength, i.e. wavelength at which the S/N is calculated. [μm]

  The ETC actually calculates and plots the S/N as a function of wavelength centred on $\lambda_{\rm ref}$.

- R: Spectral resolution. Must be > 100.

  Caution: for $R > 100\,000$ the atmospheric emission and absorption are computed at a resolution of $R = 100\,000$ which may lead to unexpected and inaccurate results. See Section 11.2 for details.

- $\Delta\lambda$: Wavelength range that is used for the integration over wavelength. [μm]

  Set equal to a resolution element: $\Delta\lambda = \lambda_{\rm ref}/R$. It is assumed that $\Delta\lambda$ is sampled by 2 spectral pixel.

- ξ: Atmospheric transmission.

  Depends on site, airmass and $\lambda_{\rm ref}$ and has two components, one due to molecular absorption and one due to scattering: $\xi = \xi_{\rm abs}\,\xi_{\rm sc}$. See Section 5.6.

- $\hat{F}_{\rm obj}$: Object flux (point source) or object surface brightness (extended source) at the telescope entrance. [W/m^2/μm or W/m^2/μm/arcsec^2]

  $\hat{F}_{\rm obj} = \xi F_{\rm obj}$.

- ϵ: Total efficiency.

  Set to 0.25. This is the ratio between the number of detected photo-electrons and the number of photons incident at the telescope entrance, i.e. it includes the telescope, instrument and detector, but excludes the atmosphere.

- E_γ: Photon energy at $\lambda_{\rm ref}$. [J/γ]

  $E_\gamma = 1.985 \times 10^{-19}/\lambda_{\rm ref}$.

- c: Total conversion factor from energy flux incident at the telescope entrance to detected number of photo-electrons. [e$^-$/s per W/m^2/μm]

  $c = \epsilon\ \Delta\lambda\ A/E_\gamma$.

- T: Detector exposure time for one exposure (DIT). [s]

- $n_{\rm exp}$: Number of exposures (NDIT).

- e: Encircled energy or fraction of PSF in the S/N reference area.

  For a point source this value is looked up in Table 11.1, 11.2 or 11.3 as appropriate for the chosen AO mode, using $R_{\rm ref}$ and $\lambda_{\rm ref}$ as input. For an extended source this parameter is not needed.

- $N_{\rm obj}$: Number of detected electrons from object in the S/N reference area per exposure. [e$^-$]

  For a point source: $N_{\rm obj} = \hat{F}_{\rm obj}\ e\ c\ T$.
  For an extended source: $N_{\rm obj} = \hat{F}_{\rm obj}\ \Omega\ c\ T$.

- $F_{\rm sky}$: Background surface brightness. [W/m^2/μm/arcsec^2]

  See Section 5.

- $N_{\rm sky}$: Number of detected electrons from the background in the S/N reference area per exposure. [e$^-$]

  $N_{\rm sky} = F_{\rm sky}\ \Omega\ c\ T$.

- $N_{\rm pix}$: Number of detector pixel over which the light from the S/N reference area is spread.

  $N_{\rm pix} = 2\ N_{\rm spec}$, where the factor 2 comes from the integration over wavelength.

- d: Detector dark current. [e$^-$/s/pixel]

  See Table 7.1.

- r: Detector read-out noise. [e$^-$/pixel]

  See Table 7.1.

- S/N: Signal-to-noise ratio per resolution element.

$$S/N = \frac{\sqrt{n_{\rm exp}}\, N_{\rm obj}}{\sqrt{N_{\rm obj} + N_{\rm sky} + N_{\rm pix}\, r^2 + N_{\rm pix}\, d\, T}}.$$

11.2 Explanations

11.2.1 The target

The target's flux is specified by giving its magnitude in any one of the allowed bands (U to Q), and its flux distribution. The latter is integrated over the chosen band and then normalised to the specified magnitude. The zero-points of the magnitude scale may be either Vega or AB (cf. Table 9.1). Together, the input magnitude and the flux distribution determine the object flux at the observing wavelength, $\lambda_{\rm ref}$ (which may also lie in the range U to Q). Normally, ESO ETCs offer the Pickles library of stellar spectra to select a flux distribution from. However, these spectra do not extend beyond the K-band. For longer wavelengths the ETC hence offers the MARCS model spectra.[1]

Alternatively, the target's flux at $\lambda_{\rm ref}$ may be specified directly in mJy.

The source geometry can be chosen to be a point source or an extended source. In the latter case the target magnitude is assumed to be a surface brightness in mag/arcsec^2.

11.2.2 The S/N reference area

The user has to specify the radius of a 'S/N reference area' in mas ($R_{\rm ref}$). This is the area on the sky over which the photons for the S/N calculation (both object and sky) are collected. So for an extended source (and the sky) the number of object (sky) photons is simply given by multiplying the target's (sky's) surface brightness by $\pi R_{\rm ref}^2$. For a point source, on the other hand, only some fraction of the object's flux will fall within the S/N reference area. For a given area this fraction depends on the PSF and hence on the chosen AO mode: Seeing limited (i.e. no AO), Ground Layer AO, or Laser Tomography AO. For a given AO mode and observing band the fractional energy encircled by the S/N reference area is obtained from a look-up table. The tables for the various AO modes are reproduced in Tables 11.1, 11.2 and 11.3, and are presented graphically in Figs. 11.1, 11.2 and 11.3. The values in these tables were measured from simulated PSFs described in Section 8. All PSF simulations assume a DIMM seeing of FWHM = 0.8 arcsec at 0.5 μm and a 42 m telescope. Note that we do not have simulations for an 8.2 or 30 m telescope, which can also be chosen by the user. Hence, making these choices for the diameter affects only the photon collecting area, but *not* the PSF. Similarly, the PSFs do not change when selecting different sites or airmasses. Finally, we note that the E-ELT is likely to offer AO modes other than those listed above, such as Multi-Conjugate AO or Extreme AO. Currently, we lack appropriate PSF simulations to properly include these AO modes in the ETC. However, in the case of MCAO it is probably not too unreasonable to assume similar performance as for LTAO.

The user also has to specify the number of individual spectra over which the light collected in the S/N reference area is distributed, i.e. the number of pixels perpendicular to the dispersion direction over which the light at a given wavelength is spread. Often this is identical to the number of spatial elements (spaxel) in the S/N reference area. In that case the size of a spaxel on the sky is simply given by: $\Omega_p = \pi R_{\rm ref}^2 / N_{\rm spec}$ (in mas^2 per spaxel).

The final S/N is calculated per spectral resolution element, i.e. the object's (and the sky's) light is integrated over $\Delta\lambda = \lambda_{\rm ref}/R$, where R is the spectral resolution. The ETC assumes that $\Delta\lambda$ is sampled by two pixels.

To summarise: given an object's magnitude (point source) or surface brightness (extended source) the size of the S/N reference area determines either an 'aperture correction' for a point source or the area

[1] Kindly supplied by N. Ryde of Uppsala Observatory. See http://marcs.astro.uu.se/ for details. Note that the Pickles spectra have a resolution of $R \sim 500$ and the MARCS spectra $R = 20\,000$.

over which an extended source's light is collected. It also determines the number of sky photons. Note that it does not make sense to select a value for $R_{\rm ref}$ that is smaller than the radius of the PSF's diffraction limited core (DFC) in the band of observation. That is why the DFC for each band is marked in the ETC's drop-down list of $R_{\rm ref}$ values. $N_{\rm spec}$ determines the number of detector pixels over which the light collected from the S/N reference area is spread: $N_{\rm pix} = 2N_{\rm spec}$, where the factor 2 comes from the integration over wavelength. Hence, $N_{\rm spec}$ determines the readout noise and dark current.

Usually, in instrument-specific ETCs, the parameters $R_{\rm ref}$ and $N_{\rm spec}$ are fixed by the instrument and/or the ETC developer. Giving the user control over these parameters provides a large amount of flexibility, so that different instrumental characteristics can be dealt with. The following is a list of examples of how to choose $R_{\rm ref}$ and $N_{\rm spec}$ in various situations.

- IFU:
  Here Ω_p is the size of a spaxel on the sky in mas^2, as defined above, and we assume that each spaxel produces exactly one spectrum on the detector. Ω_p should be taken from the specifications of the particular instrument you are considering.
  - point source:
    Choose $R_{\rm ref}$ = size of the PSF in the band you are observing in.
    $N_{\rm spec} = \pi R_{\rm ref}^2/\Omega_p$.
  - extended source, S/N in a single spectrum:
    $R_{\rm ref} = \sqrt{\Omega_p/\pi}$.
    $N_{\rm spec} = 1$.
  - extended source, total object S/N:
    $R_{\rm ref}$ = size of object.
    $N_{\rm spec} = \pi R_{\rm ref}^2/\Omega_p$.
- CODEX, point source:
  $R_{\rm ref}$ = size of entrance aperture (something large so that flux loss is small).
  $N_{\rm spec} = 280$.
  The number for $N_{\rm spec}$ was taken from a preliminary design of CODEX. In this design the object's spectrum is spread over 70 pixel at a given wavelength. This number has to be multiplied by 2 because there will be two cameras (at a given wavelength). Furthermore, CODEX will sample a resolution element with 4 pixel, not with 2 pixel as the ETC assumes. Hence another factor of 2 is applied to correct for this.
- Classical long-slit spectrograph:
  In this case the S/N reference area is quasi-rectangular, contrary to the ETC's assumption of a circular S/N reference area. However, for an extended source the ETC can easily be 'tricked' into doing the correct thing. Here w is the slit width and Ω_p is the linear size of a pixel on the sky, both in mas.
  - extended source, S/N in a single spectrum:
    $R_{\rm ref} = \sqrt{w\,\Omega_p/\pi}$.
    $N_{\rm spec} = 1$.
  - extended source, total object S/N:
    $R_{\rm ref} = \sqrt{w\,(\text{size of object})/\pi}$.
    $N_{\rm spec} = (\text{size of object})/\Omega_p$.
  - point source:
    Unlike the above, this case cannot be represented exactly. In the previous case (long slit + extended source) the geometry of the S/N reference area is irrelevant but in the present case it is not, and one is left with two imperfect alternatives for $R_{\rm ref}$:
    1. $R_{\rm ref} = \sqrt{w\,(\text{size of PSF})/\pi}$. With this choice the ETC will calculate the correct number of sky photons but most likely it will get the aperture correction wrong, and therefore it will use the wrong number of object photons.
    2. One chooses $R_{\rm ref}$ such that the aperture correction equals the expected or intended slit

loss. In this case the ETC will use the correct number of object photons, however, it will likely estimate the wrong number of sky photons.
The only solution is to run both of the above options with the 'Detailed S/N Info' box checked in order to obtain all the relevant numbers, and then to manually correct the number of either the object or sky photons to derive the correct result.

11.2.3 Cautionary remark

Note that the atmospheric thermal emission and atmospheric absorption spectra used by the ETC were pre-computed – they are *not* generated by the ETC on the fly. The pre-computed spectra have a spectral resolution of $R = 100\,000$. Therefore, when the user selects $R > 100\,000$ it is impossible for the ETC to compute the atmospheric emission and absorption spectra at the correct resolution. Instead the ETC is forced to use these spectra at their 'native' resolution. In this case the S/N calculated by the ETC may be inaccurate at some wavelengths.

References

Bessel M.S., Castelli F., Plez B., 1998, A&A, 333, 231
Boccas M., 2004, Gemini Newsletter, 29, 9
Cohen M., Walker R.G., Barlow M.J., Deacon J.R., 1992, AJ, 104, 1650
Cox A.N., ed., 2000, "Allen's Astrophysical Quantities", pp. 386–387
Cuby J.G., Lidman C., Moutou C., 2000, The Messenger, 101, 2
Ellis S.C., Bland-Hawthorn J., 2008, MNRAS, 386, 47
Giraud E., Vasileiadis G., Valvin P., Toledo I., 2006, arXiv:astro-ph/0611262
Hanuschik R.W., 2000, A&A, 407, 1157
Le Louarn M., Verinaud C., Korkiakoski V., Fedrigo E., 2004, Proceedings of the SPIE, 5490, 705
Le Louarn M., Verinaud C., Korkiakoski V., 2005, Comptes Rendus - Physique, 6, 1070
Oke J.B., 1974, ApJS, 27, 21
Rousselot P., Lidman C., Cuby J.-G.,Moreels G., Monnet G., 2000, A&A, 354, 1134
Schneider D.P., et al., 2007, AJ, 134, 102
Tokovinin A., 2002, PASP, 114, 1156

Table 11.1: Encircled energies for seeing limited case (no AO). These values were derived from the PSF simulations described in Section 8. In each band the red number marks the size of the diffraction limited core. Hence the numbers above the red values are not overly useful or even meaningful.

$R_{\rm ref}$	Percentage of energy enclosed in the S/N reference area											
[mas]	U	B	V	R	I	J	H	K	L	M	N	Q
2.2	0.00229	0.00263	0.00282	0.00325	0.00380	0.00480	0.00474	0.00646	0.0142	0.0367	0.160	0.0867
2.6	0.00322	0.00362	0.00396	0.00460	0.00529	0.00663	0.00664	0.00908	0.0201	0.0512	0.223	0.121
3.3	0.00519	0.00582	0.00640	0.00737	0.00857	0.0107	0.0110	0.0146	0.0331	0.0824	0.359	0.195
4.2	0.00843	0.00934	0.0104	0.0119	0.0140	0.0174	0.0180	0.0236	0.0531	0.134	0.582	0.316
5.0	0.0119	0.0132	0.0147	0.0169	0.0199	0.0245	0.0260	0.0348	0.0758	0.188	0.825	0.448
5.4	0.0139	0.0154	0.0171	0.0198	0.0233	0.0283	0.0306	0.0410	0.0881	0.219	0.962	0.523
7.5	0.0268	0.0295	0.0328	0.0384	0.0451	0.0540	0.0619	0.0828	0.167	0.405	1.83	1.01
9.9	0.0468	0.0512	0.0572	0.0670	0.0775	0.0950	0.114	0.150	0.289	0.683	3.10	1.76
10.0	0.0478	0.0523	0.0584	0.0685	0.0792	0.0968	0.116	0.153	0.290	0.700	3.14	1.79
13.0	0.0809	0.0886	0.0982	0.115	0.133	0.167	0.202	0.265	0.488	1.13	4.98	3.03
15.0	0.108	0.118	0.131	0.152	0.177	0.224	0.271	0.355	0.634	1.47	6.30	4.02
20.0	0.192	0.209	0.234	0.270	0.316	0.397	0.493	0.623	1.10	2.38	10.3	6.84
21.0	0.212	0.231	0.258	0.298	0.348	0.437	0.544	0.683	1.20	2.56	11.4	7.42
29.0	0.403	0.441	0.493	0.567	0.660	0.826	1.02	1.27	2.23	4.27	18.8	12.6
50.0	1.19	1.30	1.46	1.67	1.94	2.42	2.93	3.76	6.44	9.94	30.3	32.0
63.0	1.88	2.06	2.31	2.64	3.06	3.79	4.59	5.86	9.55	14.3	33.7	41.2
100.0	4.66	5.08	5.68	6.47	7.46	9.13	11.0	13.7	20.2	27.0	47.8	55.1
120.0	6.63	7.21	8.04	9.13	10.5	12.8	15.3	18.6	26.8	33.8	53.5	57.0
150.0	10.1	11.0	12.2	13.7	15.7	18.9	22.3	26.7	35.8	43.4	59.9	62.3
200.0	17.1	18.4	20.3	22.7	25.6	30.1	34.7	40.1	49.8	56.4	68.7	74.7
300.0	33.5	35.6	38.5	42.0	46.1	51.8	56.8	61.9	69.5	73.7	80.4	81.2
400.0	50.0	52.4	55.5	59.1	63.0	68.0	71.9	75.6	80.5	83.0	86.4	86.5
500.0	64.0	66.1	68.8	71.8	74.8	78.5	81.2	83.6	86.7	88.2	90.0	89.7
800.0	88.0	88.3	88.9	89.8	90.7	91.8	92.6	93.3	94.2	94.6	94.9	94.1
1000.0	94.5	93.9	93.8	94.0	94.3	94.8	95.2	95.6	96.1	96.3	96.3	95.6

Table 11.2: Encircled energies for GLAO. These values were derived from the PSF simulations described in Section 8. In each band the red number marks the size of the diffraction limited core. Hence the numbers above the red values are not overly useful or even meaningful.

$R_{\rm ref}$	Percentage of energy enclosed in the S/N reference area											
[mas]	U	B	V	R	I	J	H	K	L	M	N	Q
2.2	0.00278	0.00319	0.00376	0.00446	0.00594	0.00957	0.0136	0.0310	0.234	0.449	0.303	0.104
2.6	0.00390	0.00446	0.00530	0.00635	0.00836	0.0131	0.0189	0.0426	0.325	0.627	0.424	0.145
3.3	0.00631	0.00716	0.00844	0.0103	0.0132	0.0211	0.0306	0.0674	0.497	1.000	0.683	0.234
4.2	0.0103	0.0115	0.0135	0.0168	0.0217	0.0338	0.0495	0.108	0.761	1.56	1.11	0.378
5.0	0.0145	0.0163	0.0190	0.0236	0.0303	0.0467	0.0695	0.150	1.03	2.13	1.57	0.536
5.4	0.0169	0.0191	0.0222	0.0275	0.0353	0.0546	0.0805	0.173	1.16	2.45	1.83	0.626
7.5	0.0324	0.0365	0.0431	0.0522	0.0677	0.102	0.158	0.318	2.08	4.17	3.52	1.21
9.9	0.0566	0.0629	0.0743	0.0909	0.117	0.175	0.276	0.524	3.18	6.78	5.88	2.10
10.0	0.0577	0.0642	0.0758	0.0928	0.119	0.179	0.280	0.539	3.20	6.93	5.94	2.15
13.0	0.0975	0.109	0.128	0.156	0.198	0.297	0.471	0.866	4.29	10.4	9.31	3.63
15.0	0.130	0.145	0.170	0.209	0.263	0.393	0.624	1.14	4.97	12.1	11.8	4.81
20.0	0.230	0.259	0.301	0.370	0.466	0.695	1.08	1.98	6.35	15.7	19.3	8.14
21.0	0.254	0.286	0.333	0.408	0.514	0.766	1.19	2.17	6.64	16.1	21.0	8.79
29.0	0.483	0.543	0.635	0.772	0.970	1.44	2.15	3.83	10.2	18.8	34.2	15.1
50.0	1.43	1.60	1.87	2.26	2.84	4.09	5.94	9.41	20.1	31.7	51.0	38.0
63.0	2.25	2.52	2.94	3.55	4.45	6.30	9.00	13.7	25.6	37.4	52.9	48.7
100.0	5.55	6.19	7.16	8.54	10.5	14.4	19.5	26.7	39.7	50.4	68.4	63.8
120.0	7.85	8.74	10.1	11.9	14.6	19.5	25.5	33.5	46.3	55.7	72.9	65.0
150.0	11.9	13.2	15.1	17.7	21.2	27.4	34.3	42.7	55.0	62.6	75.8	69.6
200.0	19.8	21.8	24.6	28.2	32.8	40.2	47.4	55.1	65.3	71.5	80.8	82.6
300.0	37.7	40.5	44.2	48.7	53.7	60.5	66.0	71.2	77.9	81.5	86.5	86.3
400.0	54.5	57.2	60.7	64.7	68.7	73.6	77.2	80.5	84.6	87.0	90.2	90.0
500.0	67.9	70.0	72.7	75.6	78.4	81.7	84.1	86.1	88.7	90.3	92.2	92.0
800.0	89.3	89.4	89.9	90.6	91.4	92.3	93.1	93.7	94.5	94.9	95.5	95.0
1000.0	95.0	94.4	94.2	94.3	94.6	95.0	95.4	95.8	96.2	96.4	96.6	96.1

Table 11.3: Encircled energies for LTAO. These values were derived from the PSF simulations described in Section 8. In each band the red number marks the size of the diffraction limited core. Hence the numbers above the red values are not overly useful or even meaningful.

$R_{\rm ref}$	Percentage of energy enclosed in the S/N reference area											
[mas]	U	B	V	R	I	J	H	K	L	M	N	Q
2.2	0.00400	0.00500	0.0160	0.161	0.973	3.08	4.39	4.49	2.77	1.67	0.394	0.111
2.6	0.00500	0.00700	0.0210	0.201	1.23	4.09	5.84	5.93	3.87	2.33	0.550	0.154
3.3	0.00900	0.0120	0.0310	0.265	1.63	6.06	8.79	8.82	6.06	3.76	0.886	0.249
4.2	0.0140	0.0190	0.0460	0.336	2.03	7.91	13.2	13.1	9.06	5.98	1.44	0.403
5.0	0.0200	0.0270	0.0610	0.400	2.29	9.40	15.9	17.9	12.0	8.11	2.04	0.571
5.4	0.0230	0.0310	0.0700	0.433	2.40	9.91	17.2	20.4	13.8	9.23	2.37	0.666
7.5	0.0450	0.0590	0.121	0.605	3.10	11.5	22.2	28.9	24.0	15.9	4.58	1.28
9.9	0.0780	0.102	0.193	0.787	3.78	13.5	24.1	35.4	36.0	25.4	7.67	2.24
10.0	0.0790	0.104	0.196	0.794	3.80	13.6	24.2	35.5	36.2	25.8	7.86	2.28
13.0	0.133	0.172	0.307	1.01	4.33	16.2	27.7	37.5	45.6	38.7	12.1	3.86
15.0	0.176	0.228	0.392	1.17	4.58	16.9	30.8	39.3	50.8	44.9	15.3	5.14
20.0	0.312	0.397	0.647	1.61	5.33	18.0	33.9	47.2	53.3	56.4	25.0	8.70
21.0	0.344	0.436	0.706	1.71	5.49	18.1	34.1	48.5	53.7	57.4	27.5	9.39
29.0	0.655	0.819	1.26	2.59	6.74	19.8	35.5	51.8	62.1	60.2	44.6	15.9
50.0	1.91	2.35	3.35	5.78	10.9	23.8	39.4	55.0	72.0	78.0	65.4	40.6
63.0	3.01	3.66	5.06	8.09	14.2	26.8	41.4	56.8	73.2	79.3	66.8	51.8
100.0	7.27	8.67	11.2	15.8	23.2	36.2	48.2	60.6	76.7	82.2	83.4	67.5
120.0	10.2	12.0	15.2	20.3	27.9	40.6	52.2	63.0	77.9	83.9	86.8	68.5
150.0	15.1	17.5	21.4	27.1	34.7	46.7	56.9	66.8	79.2	84.5	87.3	73.1
200.0	24.3	27.5	32.1	38.1	44.9	55.1	63.8	71.6	81.5	86.3	89.6	86.6
300.0	43.2	46.7	51.2	56.4	61.6	67.6	73.1	78.5	85.4	88.7	92.0	89.2
400.0	59.1	61.9	65.4	69.1	72.7	76.8	79.4	83.0	88.1	90.5	93.4	91.8
500.0	70.9	72.8	75.1	77.6	80.0	82.7	84.6	86.2	89.9	91.9	94.1	93.5
800.0	89.3	89.2	89.4	89.8	90.4	91.2	91.9	92.5	93.2	94.3	95.7	95.4
1000.0	94.7	93.7	93.3	93.3	93.4	93.7	94.1	94.4	94.9	95.2	96.3	96.1

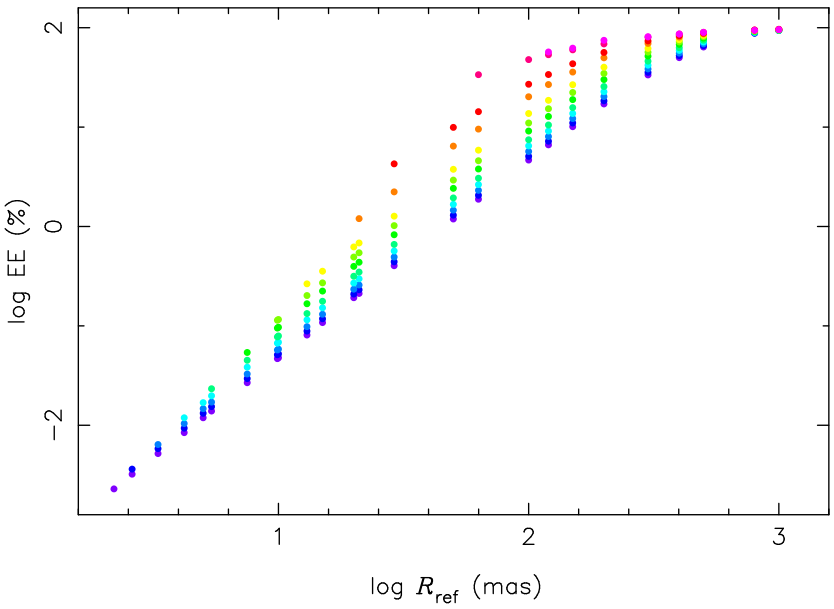

Figure 11.1: Encircled energy as a function of $R_{\rm ref}$ for no AO, i.e. a graphical representation of Table 11.1. Different bands are represented by differently coloured points. Values are only shown down to the size of the band's diffraction limited core.

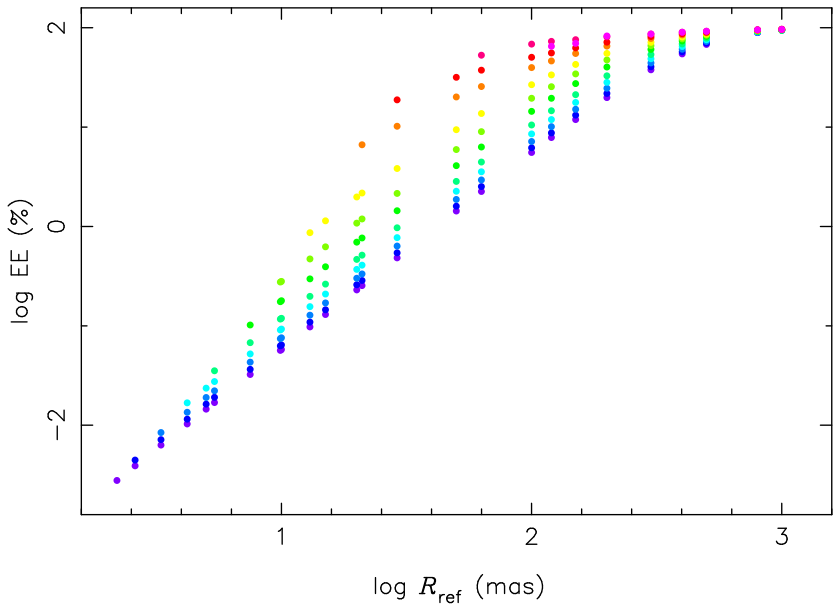

Figure 11.2: Encircled energy as a function of $R_{\rm ref}$ for GLAO, i.e. a graphical representation of Table 11.2. Different bands are represented by differently coloured points. Values are only shown down to the size of the band's diffraction limited core.

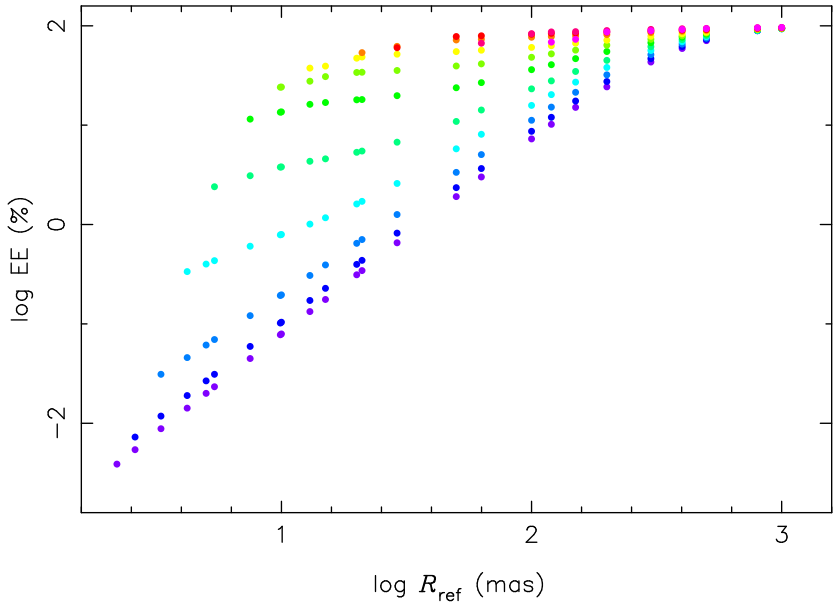

Figure 11.3: Encircled energy as a function of $R_{\rm ref}$ for LTAO, i.e. a graphical representation of Table 11.3. Different bands are represented by differently coloured points. Values are only shown down to the size of the band's diffraction limited core.